UNIVERSITI PUTRA MALAYSIA

STRUCTURAL AND OPTICAL PROPERTIES OF CHITOSAN-1,8-NAPHTHALIMIDE THIN FILM AND ITS POTENTIAL IN GLUCOSE SENSING USING SURFACE PLASMON RESONANCE

NUR IZZATI BINTI ISHAK

lp
FS 2022 68

STRUCTURAL AND OPTICAL PROPERTIES OF CHITOSAN-1,8-NAPHTHALIMIDE THIN FILM AND ITS POTENTIAL IN GLUCOSE SENSING USING SURFACE PLASMON RESONANCE

By

NUR IZZATI BINTI ISHAK

196784

Thesis Submitted to the Department of Physics, Universiti Putra Malaysia, in partial Fulfilment of the Requirements for the Degree of Bachelor of Science in Physics with Education (Honours)

January 2022

All material contained within the thesis, including without limitation text, logos, icons, photographs and all other artwork, is copyright material of Universiti Putra Malaysia unless otherwise stated. Use may be made of any material contained within the thesis for non-commercial purposes from the copyright holder. Commercial use of material may only be made with the express, prior, written permission of Universiti Putra Malaysia.

Copyright © Universiti Putra Malaysia

DEDICATION

To my beloved parents Ishak bin Osman and Azizah binti Ahmad

For their unstoppable love and support

To my precious siblings and family

For their support and make my life full with happiness

To all my lovely and cheerful friends

For the memories that we had been created together and make my life complete

To all my lectures

For helping me in this journey thoroughly and the knowledge given to me

Thank you all

© COPYRIGHT UPM

ABSTRACT

STRUCTURAL AND OPTICAL PROPERTIES OF CHITOSAN-1,8-NAPHTHALIMIDE THIN FILM AND ITS POTENTIAL IN GLUCOSE SENSING USING SURFACE PLASMON RESONANCE

By

NUR IZZATI BINTI ISHAK 196784

January 2022

Supervisor: Assoc. Prof. Dr. Yap Wing Fen (PhD)

Department: Department of Physics, Faculty of Science

In this study, the preparation of chitosan-1,8-naphthalimide (Chi/Napht) has been described. The obtained Chi/Napht thin film was then characterized by using Fourier transform infrared spectroscopy (FTIR), atomic force microscopy (AFM) for structural properties and UV-Vis spectroscopy for optical properties. FTIR confirmed the functional group that excited in Chi/Napht such as carbonyl, carboxyl and hydroxyl group. Meanwhile, UV-Vis identified the absorbance value and optical band gap of Chi/Napht. The observed result was found between 220 nm to 300 nm for absorbance peak and 3.978 eV for optical band gap. Then the Chi/Napht thin film was incorporate with surface plasmon resonance (SPR) to identify its sensing potential towards glucose. The result showed positive response for

© COPYRIGHT UPM

different concentration of glucose and obtained that Chi/Napht thin film can detect glucose as low as 5 nM. The sensor produces a linear response for glucose with sensitivity of 1.0014° nM^{-1} for range 5 to 100 nM and 1.6578° $\times 10^{-4}$ nM^{-1} for 200 to 1000 nM of glucose concentration. Last but not least, AFM was used to identify the roughness of Chi/Napht thin film whereas the value was 0.179 μm before contact and 0.125 μm after the contact with glucose solution. Thus, this study is successful in determing the characteristic of Chi/Napht thin film and its potential in glucose sensing using SPR spectroscopy.

© COPYRIGHT UPM

ABSTRAK

STRUKTUR DAN CIRI OPTIK KITOSAN-1,8-NAFTALIMIDA DAN POTENSINYA DALAM PENGESANAN GLUKOSA MENGGUNAKAN SPEKTROSKOPI RESONANS PERMUKAAN PLASMON

Oleh

NUR IZZATI BINTI ISHAK 196784

Januari 2022

Penyelia: Prof. Madya Dr. Yap Wing Fen (PhD)

Fakulti: Jabatan Fizik, Fakulti Sains

Dalam kajian ini, cara penyediaan kitosan-1,8-naftalimida (Chi/Napht) telah diterangkan. Kemudian, Chi/Napht dikaji cirinya menggunakan spektroskopi inframerah transformasi Fourier (FTIR), mikroskopi daya atom (AFM) untuk ciri struktur dan spektroskopi penerapan UV-Vis untuk ciri optikal. FTIR mengesahkan kewujudan kumpulan karbonil, karboksil dan hidroksil yang wujud dalam Chi/Napht. Sementara, UV-Vis mengenalpasti nilai penyerapan dan julat jalur optik untuk Chi/Napht. Keputusan yang diperolehi di antara 220 nm hingga 300 nm untuk puncak penyerapan dan 3.978 eV untuk julat jalur optik. Seterusnya, Chi/Napht filem nipis digabungkan dengan spektroskopi resonans permukaan plasmon (SPR) untuk mengkaji

© COPYRIGHT UPM

potensinya dalam mengesan glukosa. Keputusan menunjukkan tindak balas positif terhadap larutan glukosa yang berbeza dan didapati Chi/Napht mampu untuk mengesan larutan glukosa serendah 5 nM. Sensor ini menghasilkan tindak balas linear terhadap larutan glukosa dengan nilai pertalian 1.0014° nM^{-1} untuk 5 hingga 100 nM dan 1.6578° × 10^{-4} nM^{-1} untuk kepekatan 200 hingga 1000 nM larutan glukosa. Akhirnya, AFM digunakan untuk mengkaji kekasaran permukaan filem nipis Chi/Napht, dimana nilai sebelum berhubung adalah 0.179 μm dan nilai selepas berhubung dengan larutan glukosa adalah 0.125 μm. Oleh itu, kajian ini berjaya untuk mengkaji ciri-ciri Chi/Napht dan kebolehannya untuk mengesan larutan glukosa.

© COPYRIGHT UPM

ACKNOWLEDGEMENT

First and foremost, I am very grateful to Allah Subahanahuwata'ala for providing me time, good health and strength in doing this project throughout these two semesters. Special thanks to my beloved parents, Ishak bin Osman, and Azizah binti Ahmad for their prayers, encouragement and continues support. Another big thank to my sibling Muhammad Izzat, Muhammad Zikri, and Alia Nadira for always being there for me.

I would like to express my sincere gratitude to my supervisor, Assoc. Prof. Dr Yap Wing Fen for his invaluable guidance, patient, helps, and also for his trust on my ability to complete this project. My sincere thanks also go to Dr. Nur Alia Sheh Omar for her help and cooperation with me throughout this study work. My grateful also extend to all PhD and Master students for their guidance on how to write thesis, conducting experiment, analysis data and lead me to the right track.

Also, I would like to thanks to my final year project teammates, Farah Juwairiyah, Illya Aizzah, Habibuzzikri and Faris for the great teamwork, mental support and scarification. I am also deeply grateful to have Atul Jieha, Irdina 'Amirah and all of my coursemates for the continuous support and love.

© COPYRIGHT UPM

TABLE OF CONTENT

© COPYRIGHT UPM

© COPYRIGHT UPM

LIST OF FIGURES

© COPYRIGHT UPM

LIST OF TABLES

© COPYRIGHT UPM

LIST OF ABBREVIATIONS

AFM	Atomic force microscopy
Chi/Napht	Chitosan-1,8-naphthalimide
E_g	Energy band gap
FTIR	Fourier transform infrared spectroscopy
mL	Mililiter
min	Minutes
nM	Nanomolar
RMS	Root mean square
rpm	Revolution per minute
s	Seconds
SPR	Surface plasmon resonance
UV-Vis	UV-Visible Spectrometer

© COPYRIGHT UPM

CHAPTER 1

INTRODUCTION

1.1 Chitosan

Chitosan is a semicrystalline polymer material composed of β-(1-4)-linked D-glucosamine and *N*-acetyl-D-glucosamine. Chitosan is a product derived from partial deacetylation of chitin. Chitin is the structural element easily can discover in our natural source (crabs, insect, lobster, fungal mycelia). The source of chitosan and method of isolation determine the quality of chitosan (Galed et al., 2005).

The unique characteristic of chitosan such as biocompatibility, biodegradability, good film-forming capability, good absorption capacity, non-toxicity and low cost (Wing et al., 2015). In addition, chitosan and its derivatives have high surface area, tensile strength, conductivity and can easily molded into variety shape such as into films, powder, and solution (Shukla et al., 2013). Therefore, chitosan has been widely used for different biological and biomedical application due to its special properties. Chitosan is more efficiently in absorption compared to chitin because it has a large number of amino groups on chitosan chain (Fen & Yunus, 2011).

© COPYRIGHT UPM

1.2 1,8-Naphthalimide

1,8-naphthalimide derivatives from 4-alkoxy and 4-acylamino. Aromatic rings inside the 1,8-naphthalimide sensitives to substrate. For example, amino function at the 3, 4, 5 or 6 location of the aromatic ring allows the introduction of other produce compounds. Besides, it also gives a major effect on the chemical, photochemical and spectroscopic properties such as dichroism, absorption, and fluorescence (Banerjee et al., 2013).

The optical and physical properties of the naphthalimide which are highly dependent on the structure of the aryl rings make them suitable candidates to monitor their binding to biomolecules. Due to that many 1,8-naphthalimide derivatives have been developed such as anticancer agent, as DNA targeting binders and as well-established fluorescent brightening agents (Banerjee et al., 2013). The 1,8-naphthalimide structure has a good future in the field of small targeting biomolecules in human blood; its ease of synthesis, have good photostability, possess high antitumor activity towards human and ability to modify the basic structure of 1,8-naphthalimide is the key to its achievement (Jia et al., 2014).

1.3 Glucose

Glucose or dextrose is a simple sugar that commonly can be found in human blood. Glucose is a main character in providing energy for all living organisms. For physical properties, the melting point of glucose was experimented to be 158℃, 158.2℃ or 160.4 ℃ (Slade & Levine, 1988; Hurtta et al., 2004; Wungtanagorn &Schmidt, 2001). Glucose appearance as white crystalline in room temperature (Shendurse & Khedkar, 2015) and soluble in water due to present of polar hydroxyl group (Geddes, 1969).

© COPYRIGHT UPM

For human, the normal fasting glucose level in blood is <110 mg/dL (1100 ppm). While the subject with fasting glucose concentration in the range of 110 mg/dL to 125 mg/dL (1100 ppm-1250 ppm) were classified as suffering impaired fasting glucose. For diagnosed diabetes patient, the fasting glucose concentration is ≥ 126 mg/dL (1260 ppm) (Report of the Expert Committee on the Diagnosis and Classification of Diabetes Melitus, 1997).

1.4 Surface Plasmon Resonance

Surface plasmon resonance (SPR) is a sensing device using an optical approach to monitor the changes in refraction index of material near the metal surface (within ≈ 300 nm) from the sensor surface. SPR involved phenomena of total internal reflection. When p-polarized also known as transverse-magnetic polarization (TM) light passing the prism, hit the thin film and undergoes the total internal reflection the SPR will happen.

One of the methods can excite surface plasmons, free electron which located at the boundaries between metal dan dielectric is by using the attenuated total reflection method (ATR). There are two geometry of ATR method which is Kretschmann configuration and Otto configuration (Martin et al., 1992). Kretschmann geometry is easy to setup where a metal such as gold and silver interfaced with a high refractive index prism and it is not required to shine light through the adsorbate (Pattnaik, 2005). Therefore, Kretschmann configuration commonly used in SPR application.

The first application SPR was in 1982 for detection of gas and biologic sensor (Chen & Ming, 2012). Nowadays the SPR has being widely investigated and a large number of sensing technologies have been developed (Prabowo et al., 2018). This is

© COPYRIGHT UPM

because SPR sensor is simple to prepare the sample, cost-effective, quick measurement capability, also it is label-free detection, allows real-time and has sensitive features (Fen et al., 2012).

1.5 Problem Statement

In previous, chitosan and 1,8-naphthalimide have been reported as a chemical reagent for glucose molecule binding. In 2015, Shen and co-worker found that 1,8-naphthalimide derivative is a fluorescent material that has highly selectivity and sensitivity to detect glucose in a water medium. Meanwhile, Juska and Pemble reported that chitosan is a suitable candidate for a based glucose biosensor due to the presence of an amino group on the chemical structure in 2020. Both chitosan and 1,8-naphthalimide gave a good respond on the potential of the sensor device however studies on the combination of chitosan-1,8-naphthalimide has not yet discovered, especially on their characteristic. Hence the interest of this studies is to identify the optical and structural properties of chitosan-1,8-naphthalimide (Chi/Napht).

Back to our current pandemic, people with diabetes have been considered as being a high potential risk to COVID-19 (Gupta, 2020). Therefore, self-monitoring body blood glucose is important to reduce the risk posed to COVID-19. Many alternate methods for glucose sensing have been developed and some of the example are fluorescent sensor (Mai et al., 2019), electrochemical sensor (Marie et al., 2015), optical fiber sensor (Yu et al., 2019), photoelectrochemical sensor (He et al., 2018) and SPR sensor (Menon et al., 2019). Among of theses, SPR is the most convenient method for glucose detection because it required simple sample preparations, cost-effectively capable to measure quickly and no compulsion of reference solution (Fen

© COPYRIGHT UPM

et. al., 2012) comparing to the other. However, a gold thin film of SPR has a low sensitivity toward low concentration of glucose. To overcome this, a gold thin film must be layered with suitable material such as chitosan for this study. Chitosan is widely applied in various sensing method but the used of chitosan as a based material for glucose detection in SPR is still limited due to pH sensitivity and hydrophobic of chitosan low stability (Rinaudo, 2006). Modified thin film, Chi/Napht on SPR sensing since may enhance device sensitivity towards glucose detection. Therefore, this study is to determine the potential of modified Chi/Napht thin film by using the SPR method in glucose sensing.

1.6 Research Objectives

From the problem statement stated above, the objectives of this study are:

i. To identify the optical and structural properties of Chi/Napht thin film.

ii. To determine the potential of Chi/Napht thin film in glucose sensing using SPR.

© COPYRIGHT UPM

CHAPTER 2

LITERATURE REVIEW

2.1 Structural and Optical Properties

2.1.1 Chitosan

Chitosan is a low-cost material, non-toxic and has high permeability towards the water as well as has good adhesion. Therefore, chitosan widely used in various area such as in food processing, water treatment and in the sensing device. In sensing field, it is important to acknowledge the characteristic of the chitosan that had been used, since its characteristic play an important role in the development of high sensitivity sensor device (Mukhtar et al., 2018). The characteristic involved the determination of optical gap, absorbance value and absorbance peak for optical properties. Meanwhile, for structural properties, it describes the functional group that existed, surface morphology, root mean square (RMS) roughness, thin-film thickness and so on.

Nosal et al. (2005) studied on structural properties of chitosan and the Fourier transform infrared (FTIR) result showed a peak at 3366 cm^{-1} and 1382 cm^{-1} due to NH stretching and CH_2 stretching, respectively. While the other two bonds appeared at 1153 cm^{-1} for asymmetric vibrations of C−O−C and at 1382 cm^{-1} due to CH_3 bending. Five years later which is in 2010, Singh and co-worker used scanning electron microscopy (SEM) and FTIR to identify the structural properties of chitosan. SEM displayed chitosan had a smooth and uneven surface consist of a small hole structure with a roughness value of 14.346 nm. In FTIR, different peak was observed which are

© COPYRIGHT UPM

at 3400 cm^{-1} (N−H and O−H stretching vibration), 2935 cm^{-1} (C−H vibration), 1633 cm^{-1} (amide I), 1414 cm^{-1} (symmetrical deformation mode of C−H), 1314 cm^{-1} (amide III formation) and 1076 cm^{-1} (stretching of C−H).

In the same year, Kumar et al. developed an experiment distinguished the structural properties between chitosan and chitosan derivative. In this experiment, scanning electron micrographs (SEM) found chitosan had a smooth and nonporous surface that consist of microfibrils, a dome in shape and crystallites. In addition to information of chitosan surface morphology, SEM also exhibited flat lamellar phases on which a huge number of protruding microfibrils are evident, Meanwhile for FTIR spectrum, showed band appeared at 3429 cm^{-1} correspond to a hydroxyl group (O−H). The peak at 1592 cm^{-1} due to an amino group (N−H). The last band related to an acetylated amino group of chitin.

Meanwhile, in 2019, Oh et al. expanded the research on the characteristic of chitosan by focusing on both structural and optical properties of chitosan for their study. For optical properties, Ultraviolet-Visible Spectroscopy (UV-Vis) showed that chitosan had the absorption peak wavelength at 320 nm and an absorption value of 1.6 au. For structural properties, the FTIR method displayed a peak at 3500 to 300 cm^{-1} due to the stretching vibration of the O−H group. The absorption band at 1531 and 1630 cm^{-1} can be appointed to the alkyl group of C−H bending vibration and protonated amino ($-NH_2$) group of N−H bending vibration, respectively. Another absorption band at 1059 cm^{-1} were assigned to the anti-symmetric stretching vibration of C−O−C bridges. The last band appeared at 886 cm^{-1} which correspond to the glucopyranose ring in chitosan matrix.

In 2020, Fauzi et al. carried out an experiment that identified the structural and optical properties of chitosan. For structural properties, the value of root mean square

© COPYRIGHT UPM

(RMS) roughness for chitosan thin film by using the atomic force microscope (AFM) obtained at 1.4 nm, FTIR analysis showed peak at 3386.43 cm^{-1} and 1655.48 cm^{-1} which represent the O−H group of stretching vibration and C=O stretching bond, respectively. A weaker band found at 2901.26 cm^{-1} may represent the C−H stretching. Another absorption band at 1084.47 cm^{-1} can be appointed to the C−O group (presence of carboxyl group). The other two bands at 458.22 cm^{-1} and 500.76 cm^{-1} correspond to the C−N and C−C bond, respectively. Meanwhile, for optical properties, the absorbance value and optical gap measured by UV-Vis reported had the value of 0.7 au and 4.0723 eV, respectively.

In 2021, Gasti et al. also studied on structural and its optical properties of chitosan. For structural properties, the FTIR method showed peaks of 1408 cm^{-1} and 1636 cm^{-1} due to the O-H bending vibration and C=O stretching band. The broad absorption band at 3265 cm^{-1} corresponds to O-H stretching vibration overlaps the N−H at the same region. A weaker band displayed at 2879 cm^{-1} attributed to C−H stretching of $-CH_2$ group in chitosan. For N−H stretching and bending (amide−II), the band appeared at 1552 cm^{-1}. AFM results showed that chitosan has a thickness of 0.060 mm, line roughness of 2.8 nm and 2.14 nm for area roughness. UV-Vis showed optical properties of chitosan, and it reported chitosan had an absorbance value of 1.6 au and found to be higher at UV-Vis region between 200-500 nm.

2.1.2 1,8-Naphthalimide Derivatives

1,8-naphthalimide derivative has high absorption coefficients, excellent fluorescence properties, large stokes shifts, good fluorescence and quantum yields, easy modification and, good stability (Fu et al., 2018). Therefore, it is an important

© COPYRIGHT UPM

class of compound that has been widely found in a number of areas, such as in the fluorescence-based sensor of biology, as a colorant in the polymer industry, as organic light-emitting diodes, anticancer agents, laser dyes and electroluminescent materials. To increase the advantages application of it in each specific area, synthesis of 1,8-naphthalimide derivative had been done in previous studied. Synthesis of 1,8-naphthalimide derivatives with the other chemical compound produces a new fluorescence that differs in their characteristic.

In 2001, 1,8-naphthalimide derivatives were synthesized from amino groups, and the characteristic of this compound was reported by Grabchev and co-worker. For structural properties, FTIR showed a peak in the range of 3065 until 3077 cm^{-1} indicate the C−H stretching vibrations. The band approximately at 3240-3351 cm^{-1} represent stretching vibrations of the primary amino and bands at 3378-3513 cm^{-1} attributed to amino group (−NH). The aromatic ring deformation vibrations appeared at 774-781 cm^{-1}. A peak in the range 1346-1385 cm^{-1} was caused by imide C−N−C bonds. The characteristic bands at 1617-1625 cm^{-1} and 1578-1590 cm^{-1} correspond to stretching vibrations of C−C bonds in the naphthalene ring. Asymmetrical and symmetrical carbonyl group vibration displayed at a peak 1635-1664 cm^{-1} and 1682-1705 cm^{-1}, respectively. Meanwhile, for optical properties, UV-Vis absorption maxima at 432 nm.

Two years later which in 2003, 1,8-naphthalimide derivatives were functionalized with allyl group and their characteristic discovered by Bojinov and Grabchev. They found that 1,8-naphthalimide derivatives displayed absorption maxima at 280 nm. Meanwhile, FTIR spectroscopy showed absorption bands at 1704 and 1665 cm^{-1} due to the presence of the carboxyl group (C=O). Stretching vibrations of alkene (C=C) appeared at 1597 cm^{-1} band, and hydroxide displayed at 3460 cm^{-1} bands. This derivative also contained a C−H bond that showed an absorption peak in

© COPYRIGHT UPM

3074 and 2925 cm^{-1}. The FTIR spectra recorded bands at 1349, 3355, and 1226 cm^{-1}, respectively, which are characteristic of N−C−N, N−H and C−O−C bond.

Research on 1,8-naphthalimide derivative continued in 2009 when Zhao and co-worker studied the characteristic of bromo derivative 1,8-naphthalimide. Based on FTIR, they found peaks at 1696 and 1600 cm^{-1} due to carbonyl (C=O) stretching vibration in amide compounds. The next peak observed at 1270 and 1099 cm^{-1} represent stretching vibration C−O−C linkage. The bands at 2854, 2956, 1390, 1462 cm^{-1} were attributed to stretching vibrations of C−H in the methyl group. The characteristic bands at 1623 cm^{-1} correspond to stretching vibrations of C=C from the allyl group and a band at 563 cm^{-1} has caused by C−Br stretching. Meanwhile, UV-Vis displayed a maximum absorptions range at 431 until 436 cm^{-1}.

Next, in the year 2015, studies on the 1,8-naphthalimide derivative expanded by Refat and co-worker. They synthesized chloro derivative of 1,8-naphthalimide and the characteristic of this compound had been analyzed. Absorbance maximum peak by UV-Vis displayed a peak at 350 nm. FTIR band occurs at 1664-1706 cm^{-1} and 1661-1697 cm^{-1}, respectively, characteristic of asymmetric and symmetric carbonyl group (C=O) vibrations. Characteristic of the deformation vibrations of aromatic ring recorded a peak the bands at 778-786 cm^{-1}. The band of bending vibrational of (C−H) appeared at 1342 $cm^{-1,}$ and the stretching N−H group occurs at 1587 cm^{-1}. The absorption band displayed at 1624-1623 cm^{-1} and 1512-1527 $cm^{-1,}$ respectively, characteristic of C=C vibration.

Four years later, 1,8-naphthalimide derivatives synthesized from phenyl group reported in the year 2019 by Ren and co-worker. UV-Vis result, the absorption was found in the range of 342 to 355 nm and the absorption peak recorded at 350 nm. FTIR result showed the characteristic peaks of 1,8-naphthalimide derivatives located at 1702

© COPYRIGHT UPM

cm^{-1} for the asymmetrical carbonyl group. Meanwhile, for the symmetrical carbonyl group, it represented a peak at 1659 cm^{-1}. Absorption band at range 3200 until 3500 cm^{-1} was ascribed to the O−H vibrations of water molecules. The absorption bands around 1238-1453 cm^{-1} was attributed to deformation bands of the aromatic C−H. The last band displayed at 1593 cm^{-1} was due to aromatic carbonyl stretching vibrations.

2.2 Sensing Properties

2.2.1 Chitosan Based Composite Incorporated with the Various Method for Detection of Glucose

Recently, polymeric hydrogel (chitosan) received much attention as a material for the design of sensors. Even though chitosan exhibit good biocompatibility, a combination of chitosan with other material is still needed to overcome the poor conductivity of chitosan. Luckily modifying process can be done for chitosan due to the presence of hydroxyl and amino group in their chemical compound (Rao et al., 2016). In previous studies, synthesized chitosan derivative had been applied in the various method of glucose sensing such as in amperometry electrochemical sensor (Hossain & Park, 2016), electrochemiluminescent sensor (Wang et al., 2019) and colorimetric sensor (Maruthupandy et al., 2019). Sensing properties include a range of detection, detection limit, linear range, correlation coefficient, R^2 and sensor sensitivity.

Amperometry electrochemical glucose sensor is the first example of a glucose sensor method that used chitosan as a based material. In 2016, Hossain and Park incorporated chitosan with glucose oxide-based enzyme electrodes. A good linear correlation was obtained in the concentration range from 2 μM-10 mM, with a limit of

© COPYRIGHT UPM

detection at 2 μM. This noble nano-structured electrode also exhibited a sensitivity of 61.06 μA/mMcm^2; thus, they concluded that this fabricated biosensor showed great promise in glucose sensing applications. In the same year, bioelectrode chitosan/polypyrrole-nanotubes and gold nanoparticles nanocomposites (Chi/PPy-NTs/Au-NPs) was designed by Sharma and Kumar. This biosensor responded to glucose in the detection range from 0 to 3.2 mM, with a sensitivity of 149 μA/mMcm^2 and a low detection limit of 3.1 μM. Therefore, the designed composite film electrode, Chi/PPy-NTs/Au-NPs provided a good sensing platform for glucose.

The second example of a glucose sensor that used chitosan is the voltammetry electrochemical glucose sensor. In 2017, Uwimbabazi et al. embedded chitosan and multi-walled carbon nanotubes in the electrode of the glucose sensor. Under the optimized experimental conditions, the resulting biosensor shows a correlation coefficient, $R^2 = 0.9902$ in a linear range of 0.2 to 1.2 mM with a detection limit of 50 μM. Also, in 2017, Wang et al. fabricated chitosan onto platinum electrode surfaces of glucose sensor to serve as an adhesive layer for enzyme immobilization. This prepared material exhibited excellent performance for glucose detection with a wide linear range of 0 to 2 mM, with a sensitivity of 29.4 μA/mMcm^2 and a low limit of detection of 4.31 mM.

The third example of a glucose sensor is an electrochemiluminescent (ECL) glucose biosensor. In March 2009, Dai et al. developed a poly (diallyl-dimethylammonium chloride) (PDDA)-chitosan modified glassy carbon electrode to increase the ECL performance. This biosensor could detect glucose within a range of 0.5 to 4.0 × 10^4 nM and with a correlation coefficient of ($R^2 = 0.9988$) and a low detection limit of 0.1 nM. While in 2019, Wang and a co-worker integrated the chitosan (CS) in the wax/carbon ink-screen-printed cloth-based (PDDA-MWCNTs).

© COPYRIGHT UPM

The biosensors CS, PDDA-MWCNT showed excellent performance characteristics, including a good correlation coefficient (R^2 = 0.9986), high detection sensitivity toward glucose with a range of 0.1 to 5000 µM and a detection limit of 64 nM.

The next type of glucose sensing device is a colorimetric glucose biosensor. In 2012, Jiang et al. developed a chitosan stabilized silver nanoparticle to produce highly sensitive glucose detection. This colorimetric sensor glucose showed a detection limit as low as 100 nM in the range of 5 µM to 200 µM. The latest studies of colorimetric glucose biosensor had been reported in 2019 by Maruthupandy and a co-worker. In their studies, they cooperated chitosan with silver nanocomposites (CS/AgNCs). This developed glucose biosensor showed good linear relationship of R^2 = 0.99 in the concentration range between 0 to 100 µM and a detection limit of 5 mM.

In conclusion, there are many studies regarding the use of chitosan as a material in various glucose sensors. And most of the studies showed that applied of chitosan can increase the device sensing potential. Therefore, chitosan is a suitable material to be work within the detection of a glucose molecule.

2.2.2 1,8-Napthalimide Based Composite Incorporate with the Various Method for Biomolecule Detection

1,8-naphthalimide-based derivatives is the most promising material that most frequently used in the synthesis of fluorescent probes. It is also recognized as a special class of environmentally sensitive fluorophores that provides various design options (Geraghty et al., 2021), by modifying the substituents connected to the N-atom of the imide fragment and the 4,5- or 3,4-position of the 1,8-naphthalimide (Xie et al., 2011). Moreover, the 1,8-naphthalimide core possesses the same brightness as coumarins fluorescent (Fu & Finney, 2018) and boasting high resistance to photobleaching. There

© COPYRIGHT UPM

are studies on the use of 1,8-napthalimide for recognition biomolecules such as DNA, as well as probes for incorporation and binding to carbohydrate and for sensing of protein such as acid amino reported in the past studied.

The first example of research that used 1,8-naphthalimide derivative for the determination of biomolecule is fluorometric sensor research carried out by Sun et al. in 2011, They synthesized fluorescent, 4-butoxyethoxy-N-octadecyl-1,8-naphthalimide (BON) to measure the protein level in human serum albumin sample. The proposed biosensor method exhibited a good linearity range of 0.1 to 100 μM (R^2 = 0.9966) and a detection limit of 17.6 μM. Meanwhile, in 2013, Sun et al. developed a water-soluble 1,8-naphthalimide derivative for the determination of casein, a type of protein in milk. This Biuret method depicted detection limits at 3.0 nM in the range 0.1 to 10.5 μM.

A novel colorimetric and fluorescence dual-channel sensor for detection of glucose is the following example of research that used 1,8-naphthalimide derivative for determination of biomolecule. This study carried out by Shen et al. in the year 2015. They synthesized a new 1,8-naphthalimide derivative containing boronate groups and hexanoic acid. Boronic ester role as a recognition unit while l,8-naphthalimide represented the fluorophore. For detection of glucose in 100% water, this designed sensor reached a detection limit as low as 0.3 μM and a correlation coefficient, R^2 = 0.9912 in the linear range up to 120 μM.

The next research that used 1,8-naphthalimide derivative in biomolecule sensor is research carried by Shen et al. in 2017. In their work, they developed a sensitive fluorescent,1,8-naphthalimide derivative (NAD) to determine cysteine, a type of protein in the living cell. Fluorescent, NAD covalently attached to thiol group of cysteine and exhibited a linear range from up to 80 nM with the detection limit as low

© COPYRIGHT UPM

as 25 nM and correlation coefficient of 0.9912. The next year which in 2018, the studies on used of 1,8-naphthalimide for cysteine sensor continued by Liang and co-worker. They developed a fluorescent thiol probe that short time in response, the potential of working in a wide pH range, the detection at 69 nM in the range of at 150 to 10000 nM for cysteine.

Moreover, there are studies on the used of 1,8-naphthalimide derivative for fructose sensor device reported in 2019. Fructose is a type of sugar known as a monosaccharide group of carbohydrates. In this work, Seraj et al. designed a system that has a low fluorescence emission, and when the diol is attached, it can differ and detect fructose over the other monosaccharides very well. Therefore, a naphthalimide based probe, made with a high fusion loop and a planar structure, along with the graphene oxide nanoplatelets, has been developed in this study. The result of this designed sensor displayed correlation coefficient $R^2 = 0.99$ in the linear response range covers from 70 to 30000 µM, and the detection limit is 23 µM for fructose molecule.

The last example of research that used 1,8-naphthalimide derivative for determination of biomolecule is a fluorescent probe based on 1,8-naphthalimide for nitroreductase (NTR) detection sensor. This study reported by Zhang et al. in 2020 when 4-bromo-1,8-naphthalic anhydride was used as based for NTR responsive fluorescent probe, Na−NO_2. Nitroreductase is a family of protein biomolecule that can be found in bacteria. The proposed sensor displayed a detection limit as low as 3.4 nM when being tested in bacteria, E. coli and S. aureus. It showed a good correlation coefficient, $R^2 = 0.99036$ in the range up to 5 µg/mL.

© COPYRIGHT UPM

2.3 Detection of Glucose

2.3.1 Optical Method

Various types of glucose sensors have been developed in the past and this sensor classified differently based on the method that had been used. For glucose sensor based on optical method, it measures a change in optical property due to interaction between the analyte of interest (target) and bioreceptor (material). Optical method used visible and infrared waves (Usman et al., 2018). Some examples of optical method are fluorescence, electrochemiluminescence, colorimetric, spectrophotometric, photoelectrochemical, luminescent, photoluminescence, UV-Vis, SEM, and surface-enhanced Raman spectroscopy.

The first example sensor that used optical method in glucose sensing is colorimetric glucose sensor. In 2015, there are few researches were reported on colorimetric method for glucose monitoring. In February, Lin et al. synthesized nitrogen-doped graphene quantum dots, (N-GQDs)-catalyzed for colorimetric sensing. This sensing showed a 16 μM of detection limit and 25 to 375 μM linear range of glucose. Meanwhile in March, Li et al. combined the catalytic reaction of glucose oxide and carbon coated magnetite nanoparticle (Fe3O4@C) for developed nanomaterials-based enzymatic mimics. The use of this nanomaterial in colorimetric glucose sensor displayed a linearity range of 6 to100 μM and detection limit of 2 μM. Later in April, Wang et al. developed a selective colorimetric glucose sensor by using glucose oxidase and stable copper nanoparticles, Cu NPs-catalyzed that reached detection limit as low as 6.86 μM in the linear range of 1 to 100 μM.

Electrochemiluminescence (ECL) is the next example of glucose sensing that used the optical method in its application. There are few studies of electrochemiluminescence glucose sensing were found in 2017. Firstly, in January,

© COPYRIGHT UPM

Lou et al. developed an electrochemiluminescence biosensor for sensitive detection of glucose by the combination of glucose oxidase (GOD), Au nanoparticles (AuNPs) and assembledpolyaniline (PANi). This constructed ECL biosensor showed a wide concentration range at 0.1 to 100 µM and an extremely low detection limit of 0.05 µM for glucose. In February, Jiang et al. synthesized glucose oxidase-immobilized carbon nitride-supported Au nanocomposites (Au-g-C_3N_4) for electrochemiluminescent glucose biosensor. This proposed biosensor achieves a wide linear range of 0.1 to 8000 µM and a low detection limit at 0.05 µM.

Next example for sensing of glucose based on the optical method is photoluminescent. Few photoluminescent technologies reported in 2018. The first study, Gosh et al. (2018) worked on Al-doped ZnO (AZO) thin film and its application on photoluminescent glucose sensor. The detection limit for the enhancement of Al-doped ZnO with photoluminescent glucose sensor was at 20 µM, and the linear range was at 20 µM to 20 mM. The second study, Gosh et al. (2018a) developed a Si nanowire (NWs) and determined its application to detect glucose by photoluminescent technology. Si nanowires (NWs) can detect as low as 1.06 µM, and the linear range was 0.1 to 50 mM (correlation coefficient, R^2=0.97).

Photoelectrochemical (PEC) is another example of optical method for the detection of glucose molecule. In 2019, Zhang et al. revealed the studies on photoelectrochemical glucose sensor molecule with the help of graphitic carbon nitride (g-C_3N_4/$ZnIn_2S_4$). Combination of better photoactive material, g-C_3N_4/$ZnIn_2S_4$ proposed a linearity from 1 until 10000 µM (correlation coefficient, R^2 = 0.996) with low detection at 16 mM for glucose. In the same year, Wang et al. 2019 fabricated nonporous bismuth vanadate ($BiVO_4$) electrode on Fluorine doped tin oxide (FTO-coated glass) for photoelectrochemical biosensor. Sensing mode of this purpose for

© COPYRIGHT UPM

glucose detection displayed a dynamic detection range up to 5 mM with a detection limit as low as 0.13 µM and a good correlation coefficient, $R^2 = 0.997$.

The last example of glucose monitoring that used optical method approach is fluorometric glucose sensors. Researcher in 2021, Lu et al. created fluorometric biosensor for sensitive detection of glucose by synthesized functionalized carbon nanoparticles (CNPs) through one-step of thermal pyrolysis method. This designed sensor responded toward glucose molecule in the range of 50 µM to 2000 µM with a low detection limit of 10 µM. Another study in the same year, Zhou et al. synthesized photoluminescent silver nanoclusters (AgNCs) with polyethyleneimine as the stabilizer for fluorometric sensor purposed. This sensor reached detection limit (35 nM) and linear response in the concentration range from 0.1 to 20 µM ($R^2 = 0.9953$).

2.3.2 Surface Plasmon Resonance

Surface plasmon resonance (SPR) sensor is one of optical sensors commonly used for biomolecule detection. Excitation of surface plasmon wave occurs at the interface between a dielectric and thin film resulting in change of refractive index. For glucose detection, SPR sensor with gold thin film itself cannot measure the change of refractive index. Therefore, biochemical modification of the surface SPR thin film is required to increase the SPR sensing performance. There are studies on modification of thin film reported in previous, and each modification displayed a different result in term of a range of detection, detection limit, sensitivity, time response, pH range and correlation coefficient, R^2.

First example of modification SPR thin film is in 2010, Tian et al. developed a gold thin film combination of polypyrrole and glucose oxidase (PPy-GOx) to enhance

© COPYRIGHT UPM

SPR sensitivity. The enzymatic catalytic activity responded to the change of refractive index PPy-GOx thin film and change in SPR signal. The sensor showed a sensitivity of 0.5 μM. The linear response of the sensor is found to be between 1-100 μM. Next in 2012 Srivastava et al. fabricated SPR glucose sensor by chromium (Cr) coated and immobilizing glucose oxidase (GOx) thin film. From the experiments, a linear relationship was obtained in the range 0 to 14 mM between glucose concentration and the sensitivity found at 0.0366 nm/(mg/dL)

Next study of SPR glucose sensor is based on enzyme-induced growth of gold nanoparticles (AuNPs) reported by Bourigua et al. in 2013. This sensor designed based on biocatalytic growth of Au nanoparticles. The linear range of the sensor was found to be 0.01-7 mM with detection limit as low as 10 mM. Another study of SPR glucose sensor developed by Halim et al. in 2015. They developed SPR sensor that worked in spectral interrogation scheme. This biosensor presented a sensitivity of 0.14 nm/(mg/dL), and the detection limit 0.4 mM in the linear range of 0 to 11.1 mM.

In 2017, Yuan et al. created SPR biosensor based on glucose sensitive membrane (GSM) that consists of glucose oxidases (GODs) on SiO_2 nanoparticles and polyacrylamide gel. The sensitivity of this SPR glucose sensor was approximately at 0.14 nm/(mg/dL) in the linear range of 0 to 4.4 mM and low detection limit at 8 μM. Also, in the same year of 2017, Li et al. modified SPR sensor by glucose/galactose-binding (GGB) protein. A good correlation coefficient $R^2 = 0.981$ showed in a linear range of 5.5 to 500 μM. Meanwhile, in 2018, Li et al. enhanced the SPR glucose sensor by immobilizing glucose oxidases into silica mesocellular foams and trapping them in a polyacrylamide gel. This SPR sensor responded to glucose within a range of 0 to 9 mM and the sensitivity of 0.0135 degree/(mg/dL). Other researchers, Yuan et al. in

© COPYRIGHT UPM

2018 modified Au nanoparticles with phenylboronic acid. This fabricated sensor had a detection limit of 5 mM in the range of 0.01 to 30 mM.

The example of SPR sensor that reported in 2019 is photonic crystal fiber D-shaped SPR glucose biosensor by Lidiya and co-worker. Tests performed of this sensor in different concentration of glucose revealed a highest sensitivity 0.83 nm/(g/L) in the 0 to 100 mM range. Next SPR sensor is D-glucose non-enzymatic plasmonic biosensor by Lobry et al. reported in the same year of 2019. This biosensor exhibited a detection limit of 0.1 µM and linear range within 1 to 100 µM. Also, in 2019, Menon et al. presented s SPR glucose sensor based on nano-laminated gold/chromium, Au-Cr K-SPR. The sensor results showed sensitivity in the 4 to 12 mM linear range and limit of detection close to 4 mM.

In 2020, Phan et al. developed prism coupler SPR non-invasive glucose. Circular birefringence measurement technique becomes a model for this SPR to produce the high-resolution non-invasive (NI) sensor. Sensing mode of this purpose for glucose detection revealed a limit of detection close to 0.5 mM with the highest sensitivity in the range up to 27.8 mM and correlation coefficient, $R^2 = 0.9904$. The latest study of SPR sensor which is in 2021, gold modified carboxyl-functionalized graphene quantum dots-based (gold/CGQDs-NCC) surface plasmon resonance by Rosddi and co-worker. The incorporation of gold/CGQDs-NCC thin film with surface plasmon resonance produced positive responses towards the glucose solutions of different concentration and it was found that the sensor produces a linear response up to 0.00753° μM^{-1} with detection limit and sensitivity of 0.005 µM and 13.296° μM^{-1}, respectively.

© COPYRIGHT UPM

CHAPTER 3

METHODOLOGY

3.1 Material and Reagents

The medium molecular weight chitosan, acetic acid, and 99% 1,8-naphthalimide were purchased from Sigma Aldrich (Saint louis, MO, USA). Glucose was obtained from R&M Marketing, Essex, U.A.

3.2 Preparation of Glucose Concentration

Firstly, a glucose solution of 5 μM was prepared by dissolving 4.955 mg of glucose in 100 mL deionized water. Then 5 μM of glucose solution was diluted with deionized water by using the dilution formula $M_1V_1=M_2V_2$ to produce various concentration of glucose solution which are 5 nM, 10 nM, 50 nM, 100 nM, 200 nM, 500 nM, and 1000 nM.

3.3 Preparation of Chitosan-1,8-Naphthalimide Solution

Firstly, 100 ml of deionized water was used to dilute 1 mL of stock acetic acid obtaining 1% acetic acid. Then, 50 mL of 1% aqueous acetic acid was used to dissolve 400 mg medium molecular weight chitosan. The solution was vigorously stirred until powdered chitosan dissolved completely in the acetic acid forming chitosan solution. For preparation of 1,8-naphthalimide, 0.197 g weight of 1,8-naphthlimide dissolved in

© COPYRIGHT UPM

10 mL of sulfuric acid and 4 mL of water. Then chitosan solution was added to 1,8-naphthalimide solution with a ratio of 4:1 and stirred to form chitosan-1,8-naphtalimide solution (Chi/Napht).

3.4 Preparation of Chitosan-1,8-Naphthalimide Thin Film

Before any coating process, glass slide (24 mm × 24 mm × 0.1 mm) bought from Germany was cleaned using acetone to remove any dirt on the surface of the glass slide. Then the glass slide first coated with a 50 nm thickness of gold thin layer by using SC7640 sputter coater machine for 67 s. For second coating process, approximately 1 mL of chitosan-1,8-naphtalimide solution was placed on the top of gold layer surface fully covering the slip to add another layer. The glass cover slip was spun at 3000 rev per min for 30 s using the Specialty Coating System, P-6708D (Inc. Medical Devices, Indianapolis, IN, USA) to produce the chitosan-1,8-naphtalimide (gold/Chi-Napht) thin film. Lastly the glass slide was left for 3 minutes at room temperature to dry. Figure 3.1 shows a basic idea of gold/Chi-Napht thin film preparation.

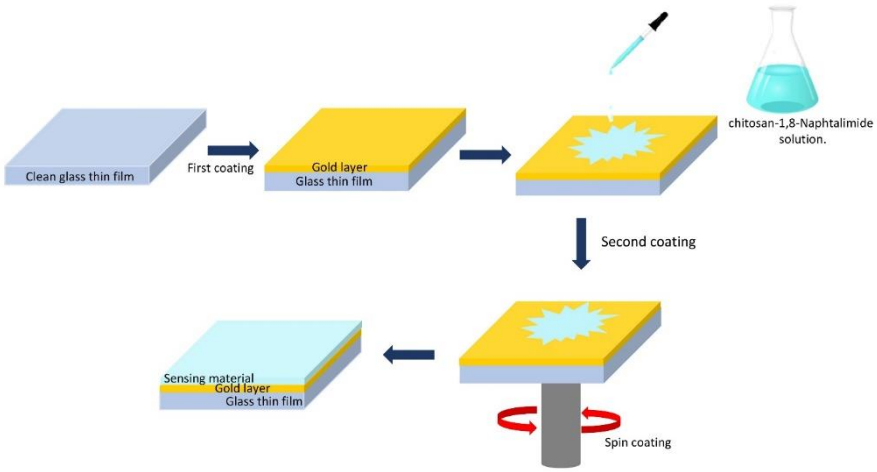

Figure 3.1: Preparation of gold-Chi/Napht thin film.

© COPYRIGHT UPM

3.5 Characterization

To characterize chitosan-1,8-naphtalimide thin film, Fourier transform infrared (FTIR) spectroscopy, atomic force microscope (AFM) and ultraviolet-visible spectroscopy (UV-Vis) and surface plasmon resonance (SPR) were used.

3.5.1 Fourier Transform Infrared Spectroscopy

Fourier transform infrared (FTIR) is a instrument to explore the physical properties of matter. More specifically, it allows the study of functional group that presence in materials (Prusty, 2019). Important component of FTIR spectroscopy is the Michelson interferometer that consist of fixed mirror, beam splitter, and mirror. Michelson interferometers provide a significant sensitivity advantage as the interferometer giving a large throughput and a higher light gathering capability (Valikyla, 2014). FTIR is widely used in polymer characterization for microscopy and imaging of rubber (Sarma, 2018), pharmaceutical analysis (Pani, 2011), forensic analysis (Maric, 2014) and food testing (Valand, 2020).

The basic operation principle of standard FTIR system involving infrared light from the beam source strikes the beam splitter and separates into two beams where half reaches a fixed mirror and half reaches a mirror. Then, these two fixed and moving mirrors reflected the beams back to the beam splitter. Recombination of these two beams constructs an interference pattern which is constructive and destructive interference. This interference pattern also known as interferogram was sent to the sample where some of the beams absorbed by the sample and some of it transmitted (passed through the sample). The transmittance and absorbance portion of the interferogram sent to a detector and presented as resulting spectrum. Absorption

© COPYRIGHT UPM

and transmission band of this resulting spectrum dedicated the functional groups of the material inside the sample. Figure 3.2 shows the working principle for FTIR.

In this study, FTIR spectrum of the modification thin films ranging from 400 to 4000 cm^{-1} were recorded using a Perkin-Elmer spectrophotometer (CA, USA).

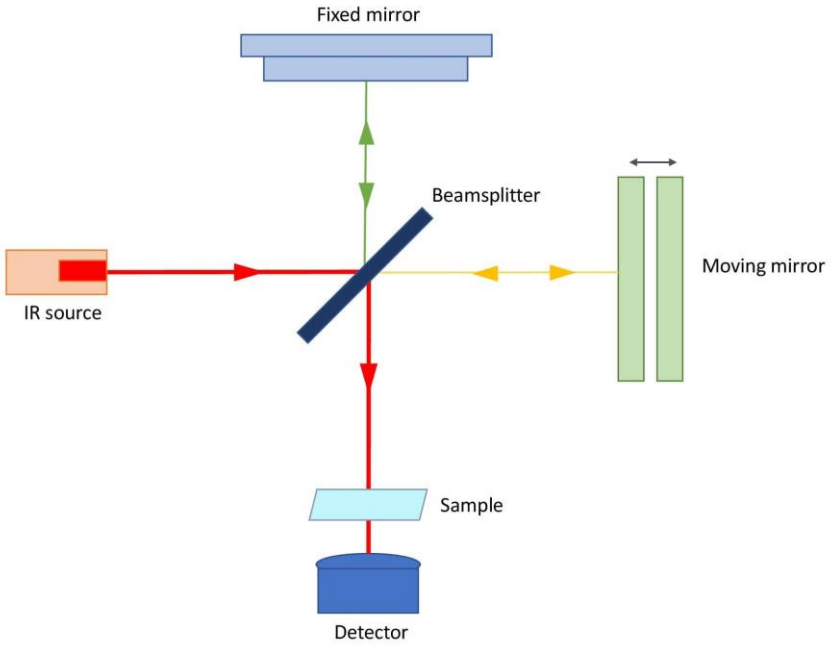

Figure 3.2: Working principle of FTIR.

3.5.2 Atomic Force spectroscopy

Atomic force microscopy (AFM) is an influential surface analysis machine that can be used to obtain high resolution nanoscale images of sample surfaces (Ray, 2013). AFM can be used for both quantitative and qualitative information, including roughness, morphology, and surface texture. For statistical analysis, it offers information on volume distributions and surface area of the sample (Farre, 2012). The AFM offers images a maximum height in the order of micrometers and a maximum

© COPY

scanning area of around 150 by 150 micrometers (Ray, 2012). Unlike scanning and transmission electron microscopy, which measures images in 2D, AFM provides image of sample in 3D.

The basic idea about how it works is AFM involves the movement of a cantilever over a sample surface. Cantilever consists of a sharp tip that is approximately 10 to 20 nm in diameter (Ray, 2013). When cantilever nearing the surface, attractive force between the tip and the surface causes the deflection of the AFM cantilever. A laser beam from the flat top of the cantilever tracked this deflection and directed into a position-sensitive photodiode (PSPD) detector**.** Any cantilever deflection will slightly cause changes in the direction of reflected beam and these changes tracked by PSPD. Interaction between reflected beam and photodiode results in electrical potential, which is useful information to generate the three-dimensional topographic image of sample surface.

In this work, the surface morphology of Chi/Napth thin film was analyzed using atomic force microscopy (Q-scope 250, Quesant Instrument Corporation) in intermittent mode to obtain high resolution of result.

3.5.3 UV-Visible Spectroscopy

Ultraviolet-visible spectroscopy (UV-Vis) is a technique that used to study the optical properties of the sample. It is a type of spectroscopy which involved the determination of a light beam intensity after it passes through a sample or reflects back from a sample surface**.** The principle of UV-Vis is based on the absorption of visible light or ultraviolet light by sample molecule, which results in the production of spectrum (Pentassuglia, 2018).

© COPYRIGHT UPM

A light from tungsten filament (radiation source) separated into different wavelengths after passed through the monochrometer and forming a single wavelength. Next, this single wavelength spilled into two beams equal in intensity before it reaches destination. One beam passed through the sample part containing material that being studied, another one beam passed through the reference part containing solvent only. The intensities of these two light beams are then measured by photodiode detectors at the same time. The intensity of the reference beam, which should have 100% Transmission (zero light Absorbance) is known as I_0. Meanwhile, the intensity of the sample beam is known as I. For intensity of sample beam (I), if the sample compound does not absorb light, it gives a result as I will be equal to I_0, ($I = I_0$) and if the sample compound absorbs light then I will be less than I_0, ($I < I_0$).

In this study, UV-VIS NIR spectrophotometer (UV-3600) from Shimadzu (Kyoto, Japan) was used to determine the absorbance, maximum wavelength or absorption peak and optical band gap energy of the sample in the range of 220-900 nm at room temperature.

3.5.4 Surface Plasmon Resonance

Surface plasmon resonance (SPR) instruments use an optical method for monitoring the refractive index near a sensor surface. In SPR there are two metal which commonly used as a component for thin film which is gold and silver. Between this two, gold reported as a best metal for SPR thin film compared to silver. This is because, gold provides more chemical interaction so therefore silver has become a thin film standard in SPR (Schasfoort, 2008). There are two types of SPR configuration which is Otto configuration and Kretschmann configuration. Most commonly use is

© COPYRIGHT UPM

Kretschmann configuration, where target material and thin film (silver and gold) deposited on the base of prism glass (Vinogradov, 2018)

Working principle for SPR sensor is when p polarized light through a prism on a sensor chip, reflection and refraction occurred. After some time, when p polarized light had bigger incident angle than the critical angle, total reflection occurred instead. Incident light that directed to and reflected from metal film (act as mirror) excite the surface plasmons causing the change in intensity as well as angle of incidence. If binding between thin film and target occurs, the refractive index will increase causing SPR reflectivity curve shift to the right. This is how SPR detect the low and high concentration of the sample. Figure 3.3 shows experiment setup for SPR technique.

In this work, SPR experiment was carried out by injecting 3 mL concentration of glucose inside the chamber. The change of resonance angle and SPR curve resulting from binding of glucose molecule with gold/Chi-Napht thin film were monitored and recorded. This process was repeated by using different concentration of glucose which 5 nM, 10 nM, 50 nM, 100 nM, 200 nM, 500 nM, and 1000 nM.

© COPYRIGHT UPM

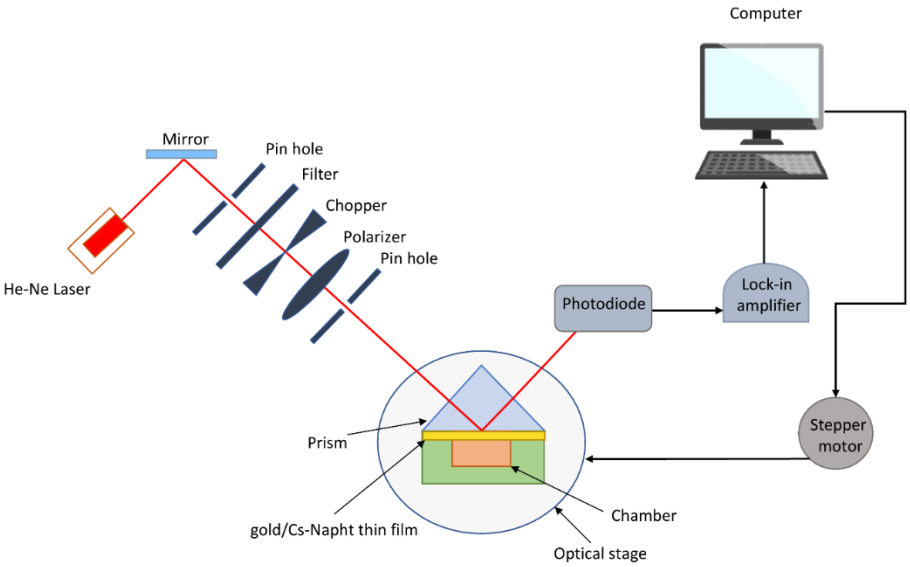

Figure 3.3: Experiment setup for SPR technique.

© COPYRIGHT

CHAPTER 4

RESULTS AND DISCUSSION

4.1 Introduction

In chapter 4, it will discuss and review the results obtained from the sample prepared using the methodology stated in previous chapter. The result of the functional group that excited in chitosan-1,8-naphthalimide (Chi/Napht) was discovered using Fourier transform infrared spectroscopy (FTIR). Next, absorption and optical band gap for optical studies were identified by using ultraviolet-visible spectroscopy (UV-Vis). The sensing potential of Chi/Napht towards glucose was determined using SPR spectroscopy. Lastly, the structural and morphology properties of Chi/Napht was discovered using atomic force microscopic (AFM).

4.2 Fourier Transform Infrared Spectroscopy Analysis

Fourier transform infrared spectroscopy (FTIR) was used to study the functional groups existed in chitosan thin film, 1,8-naphthalimide thin film, and Chi/Napht thin film. Figure 4.1 shows IR spectrum of each sample in the range of 500 cm^{-1} to 4000 cm^{-1}. For FTIR, a graph of the intensity of emission against transmitted frequencies was plotted, and each peak of the graph determined the functional group that excited on the sample.

© COPYRIGHT UPM

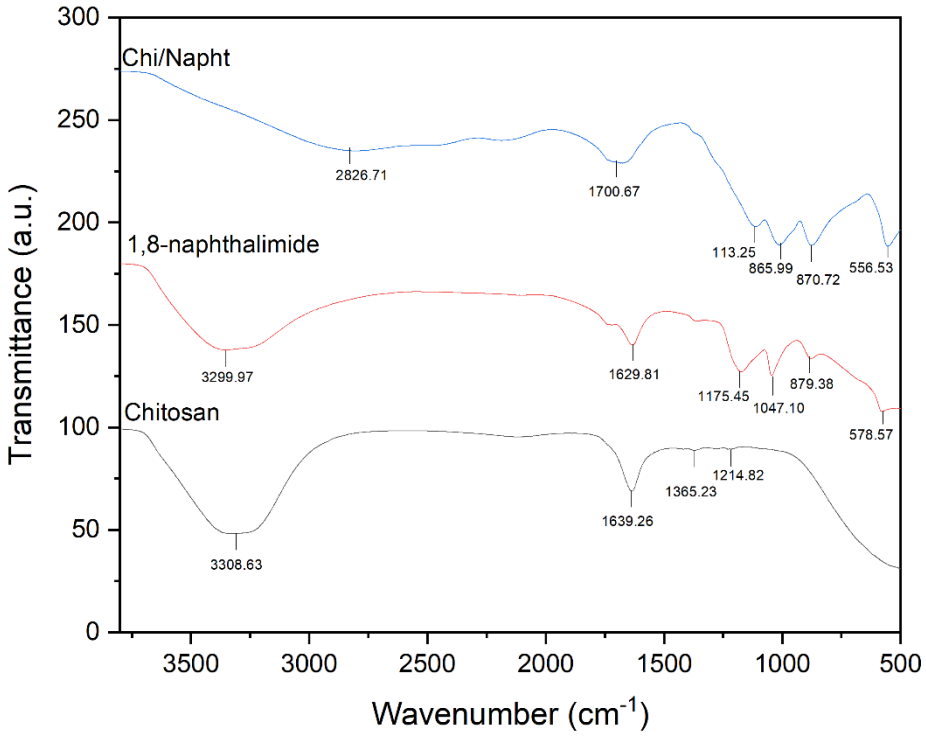

Figure 4.1: Graph of IR spectrum for chitosan, 1,8-naphthalimide and Chi/Napht solution.

In IR spectrum of chitosan thin film, board absorption band appeared at 3308.63 cm^{-1} due to presence of O−H group. While another two peaks at 1639.29 cm^{-1} and 1365.23 cm^{-1} were originated from C=O stretching bond indicated the presence of the carboxylic group in chitosan thin film. The absorption band at 1365.23 cm^{-1} appointed to a weaker C−H bond. In this study, the result for chitosan spectrum matched the FTIR result from previous study by (Anas et al., 2019).

Next for the spectrum of 1,8-naphthalimide thin film showed board absorption band at 3299.97 cm^{-1} due to the stretching vibration of O−H. The peak at 1629.81 cm^{-1} corresponded to the C−O stretching bond. Another two band at 1175.45 cm^{-1} and 1047.10 cm^{-1} can be assigned as C−H bond. Then the peak that located at 879.38 cm^{-1}

^{1} corresponds to benzene group that presence inside chemical structure of 1,8-napthalimide. A peak that reported at 578.57 cm^{-1} represents the C−C stretching bond inside naphthalene ring (Grabchev et al., 2001).

The spectrum of Chi/Napht thin film displayed quite similar properties of combination between chitosan and 1,8-naphthalimide spectrum whereas C=O bond that indicated the presence of the COOH can be found at 1700.67 cm^{-1}. Another two peak at 2826.71 cm^{-1} and 113.25 cm^{-1} correspond to C−H and C−O stretching bond, respectively. In addition, Chi/Napht spectrum also showed peaks at 865.99 cm^{-1} and 870.72 cm^{-1} due to the presence of benzene ring inside 1,8-napthalimide and a peak that appeared at 556.53 cm^{-1} was due to presence of the C−C stretching bond of naphthalene ring. In conclusion, the functional group of Chi/Napht included carboxylic acids, carboxyl and hydroxyl was identified in this study as shown in Table 4.1.

Table 4 1: Characteristic frequencies of Chi/Napht thin film.

Wavenumbers (cm^{-1})	Band assignment
2826.71	C−H stretching
1700.67	C=O stretching
1113.25	C−O stretching
865.99	Benzene ring
870.72	Benzene ring
556.53	C−C stretching

© COPYRIGHT UPM

4.3 UV-Vis Analysis

Thin films were investigated by using UV-Vis NIR spectrophotometer to identify the absorbance spectrum of the sample with wavelength ranging from 220 to 500 nm. The absorbance spectrum for chitosan, 1,8-napthalimide, and Chi/Napht are presented in Figure 4.2.

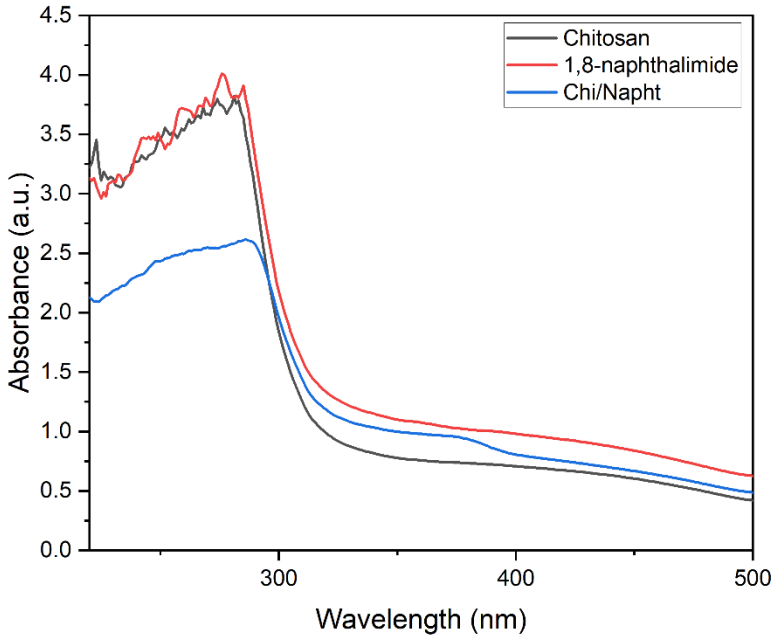

Figure 4.2: The absorbance spectrum for chitosan, 1,8-naphthalimide, and Chi/Napht thin films.

From the Figure 4.2, it shown that chitosan, 1,8-naphthalimide and Chi/Napht thin film have different absorption spectra. The UV-Vis curve for chitosan thin film displayed absorbance value of 3.82 at peak of 281 nm. The result obtained in the range of the absorption peak for chitosan that found by Anas et al (2019) which at 260 nm to 300 nm. For 1,8-naphthalimide thin film, it has absorbance value of 4.0 at wavelength 276.18 nm. Meanwhile for Chi/Napht thin film observed a lowest absorbance value of 2.61 at peak 287.54 nm. It is probably due to $\pi \rightarrow \pi^*$ bond

transition of carbonyl group (C=O) agrees with former studies that used chitosan based material (Fauzi et al., 2020).

Beer Lambert law is a theory that used to determine the UV–Vis absorbance spectrum. According to this theory, concentration of substances in solution is directly proportional to the absorbance. Beer Lambert law also describes the relationship between absorbance, A and transmittance. However, this law is applicable for monochromatic light only whereas when monochromatic light passes through a homogeneous solution, the intensity, I of the emitted radiation depends on concentration and thickness, t of sample.

The absorbance, A of samples depends on the ratio of intensities of the illumination falling on the detector in the absence I_o and the presence I_t of the sample.

$$A = log_{10} \frac{I_0}{I_t} \tag{4.1}$$

The transmittance, T of sample is given by

$$T = \frac{I_t}{I_0} \tag{4.2}$$

Absorbance and transmittance are related, thus:

$$A = log_{10} T \tag{4.3}$$

The absorbance coefficient is another quantity that can be measured. Absorbance coefficient is a very useful quantity which is used to compare samples of a varying thickness. The thickness,t of sample was obtained by using atomic force microscopy. The absorbance coefficient, α is given as

$$\alpha = 2.303 \frac{A}{t} \tag{4.4}$$

© COPYRIGHT UPM

From the equation, t is the thickness of sample in unit of meter (m). The absorbance coefficient, α is in the unit of m^{-1}. In spectroscopy, the absorbance coefficient is directly derived from the illumination of intensity of light at a specified wavelength, λ that passes through a sample (transmitted light intensity) and I_0 is the intensity of incident light.

4.3.1 Energy band gap

Energy band gap is another component that can be measured. Absorption spectra used to figure out the energy band gap of these composites. The Tauc relation is used in order to calculate the optical band gap energy from absorption spectra,

$$\alpha = \frac{k(hv - E_g)^{\frac{1}{2}}}{hv} \tag{4.5}$$

By rearrangement of the above equation

$$(\alpha hv)^2 = k(hv - E_g) \tag{4.6}$$

From the equation, photon energy is hv where h is Plank's constant, α is the absorption coefficient, E_g is the optical energy band gap, k is constant and $n = 1/2$ for direct transition. The graph of $(\alpha hv)^2$ against hv is plotted. Value of optical band gap observed from the intersection of straight line on x-axis (Abdulla & Abbo, 2012).

© COPYRIGHT UPM

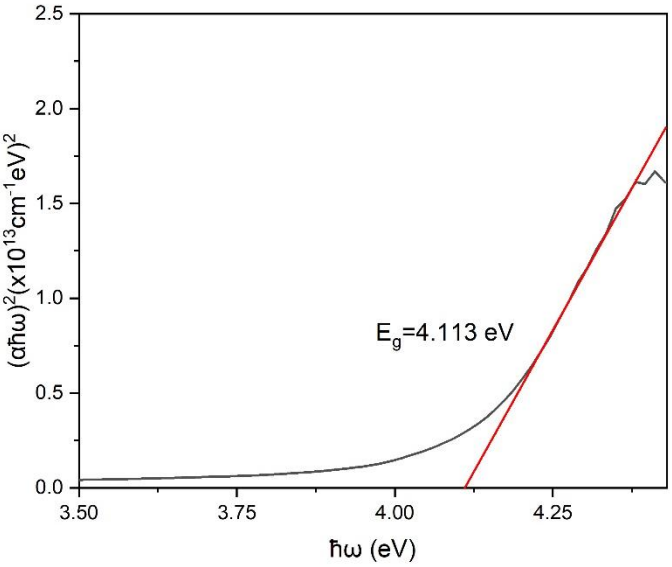

Figure 4.3: Optical band gap for chitosan thin film.

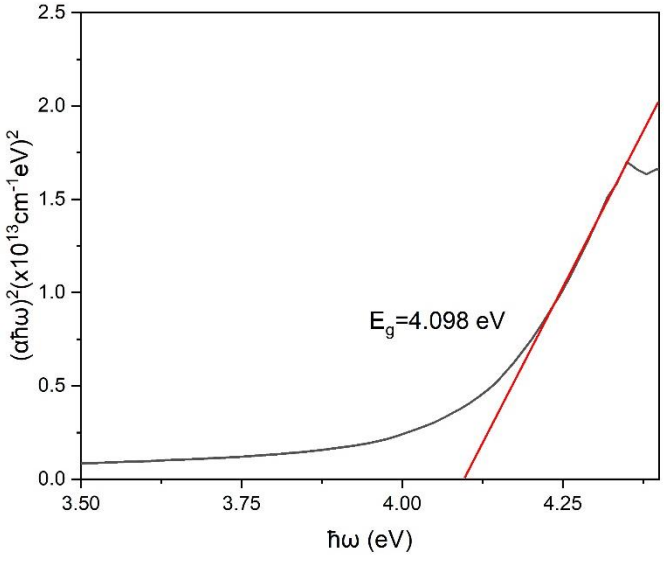

Figure 4.4: Optical band gap for 1,8-naphthalimide thin film.

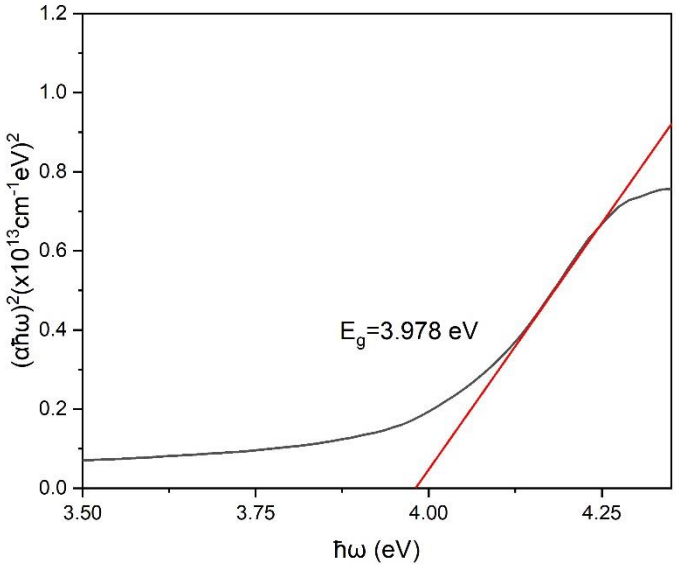

Figure 4.5: Optical band gap for Chi/Napht thin film.

Figure 4.3, Figure 4.4 and Figure 4.5 show the graph of $(\alpha hv)^2$ against hv for chitosan, 1,8-naphthalimide and Chi/Napht thin film. From the graph energy band gap for chitosan, 1,8-naphthalimide, and Chi/Napht posses a value of 4.113 eV, 4.098 eV, and 3.978 eV respectively. Based on the result, Table 4.2 represent the optical band gap for three sample. Chi/Napht thin film has a lowest value among the three samples may due to strongest interatomic spacing between atom of Chi/Napht that caused high energy needed to break the bond and caused electron moved to conduction band which decreases the optical band value (Nie et al., 2008).

Table 4.2: Optical band gap of chitosan, 1,8-naphthalimide and Chi/Napht thin films.

Sample	Optical band gap (eV)
chitosan	4.113
1,8-naphthalimide	4.098
Chi/Napht	3.978

© COPYRIGHT UPM

4.4 Sensing Properties of Thin Film

4.4.1 SPR Signal for Glucose on Gold Single Layer

A preliminary SPR test was conducted to obtain a SPR curve for gold layer in contact with deionized water. This SPR curve was used to compare the difference in resonance angle for different concentration of glucose. Also, this SPR curve also was used to compare with SPR result for sensing layer in contact with deionized water. Therefore, SPR curve for gold layer in contact with deionized water was first to be determined. To find the SPR firstly approximately 3 mL of deionized water was injected into the chamber and it was left for few minutes to ensure that interaction between deionized water (0 nM) and gold thin film complete. The SPR curve shows the resonance angle was 53.85˚ for gold in contact with deionized water as shown in Figure 4.6.

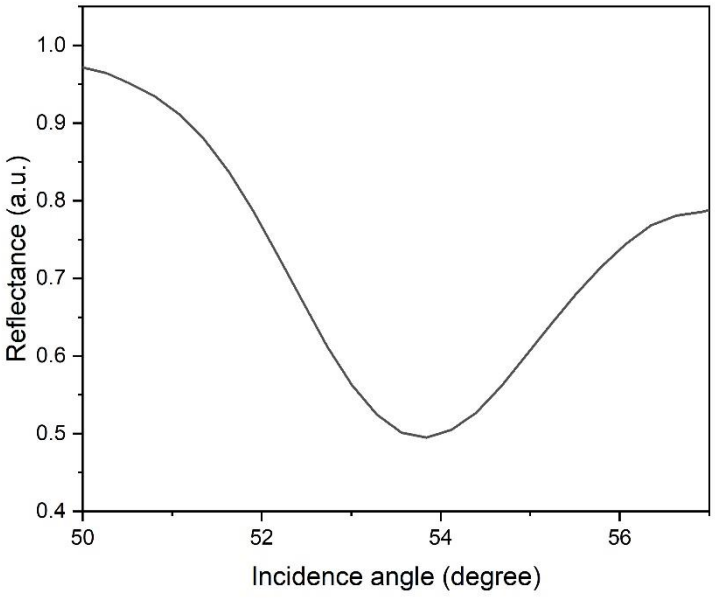

Figure 4.6: The reflectance curve for gold layer in contact with deionized water (0 nM).

Next SPR experiment was continued by using a different concentration of glucose which is 5 nM, 10 nM, 20 nM, 50 nM, 100 nM, 200 nM, 500 nM and 1000 nM. The solution injected one by one into cell starting with low concentration until high concentration. The resonance angle for all concentration of glucose compared using the SPR curve as shown in Figure 4.7. From the figure below, it obtained that SPR curve for all concentration of glucose were the same. There no shift of resonance angle from low until high concentration of glucose. This might because of in this study, low concentration of glucose was used therefore only a few molecules of glucose were able to attached to gold surface resulting the same refractive index for all concentration of glucose.

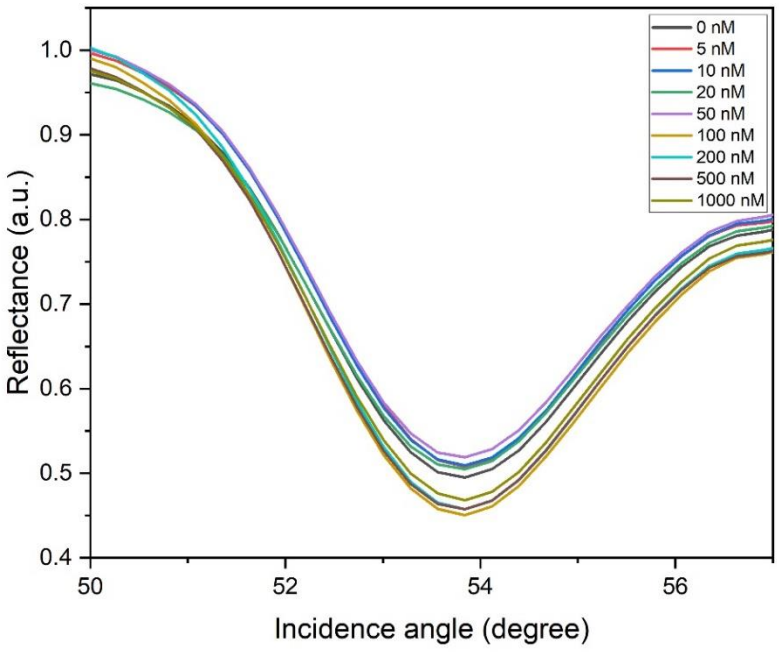

Figure 4.7: The reflectance curve for glucose (0-1000 nM) in contact with gold layer.

4.4.2 SPR Signal for Glucose using Chi/Napht on Gold Surface

The SPR experiment was continued by replaced different thin film. This replaced thin film was coated with sensing layer which chitosan-1,8-naphthalimide (Chi/Napht). This gold-Chi/Napht thin film was firstly tested with deionized water. The reflectance curve showed that resonance angle for gold-Chi/Napth thin film was 54.00° slightly higher compared to resonance angle for gold thin film which 53.83°. This changed was due to increased of reflective index when top of gold thin film coated with Chi/Napht.

To test sensing potential of gold-Chi/Napht thin film in detection of glucose the experiment was repeated with different concentration of glucose, starting with the lower concentration solution. The SPR result show that the curve slightly shifts to the left as the concentration increased as shown in Figure 4.8. This negative shift behavior might due to reduction thickness of sensing layer (Saha & Sarkar, 2016) that also affected the refractive index of thin film (Singh & Gupta, 2013) since the thickness was changed.

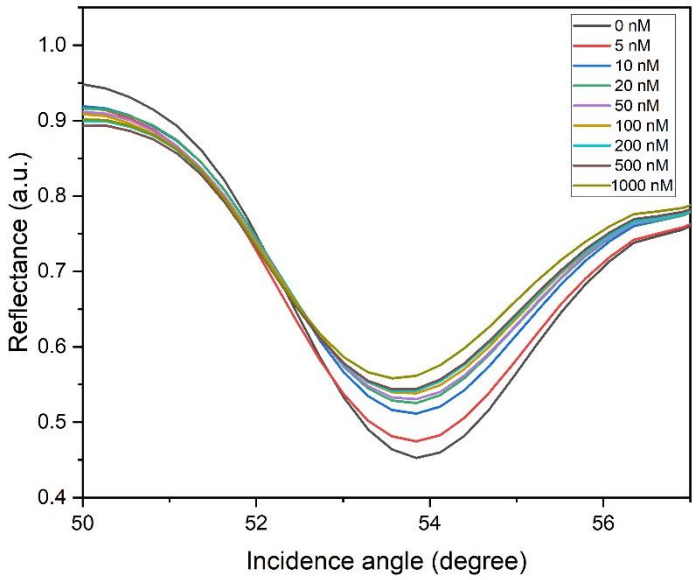

Figure 4.8: The reflectance curve for glucose (0-1000 nM) in contact with gold-Chi/Napht thin film.

4.4.3 Sensitivity of Chi/Napht Thin Film

The resonance angle shift was used as a parameter to calculate the sensor sensitivity. The value of resonance angle shift (Δθ) obtained by subtracted the resonance angle of sample with deionized water as a reference. In this study, resonance angle shift for gold and gold-Chi/Napht thin film obtained to identify the sensitivity of thin film in sensing glucose. The resonance angle shift of resonance angle for different concentrations of glucose in contact with gold and gold-Chi/Napht thin film are shown in Table 4.3.

Table 4.3: SPR resonance angle and resonance angle shift for in contact with gold thin film and gold-Chi/Napht thin film with difference concentration of glucose.

Concentration glucose (nM)	Resonance angle, θ (angle)		Resonance angle shift, $\Delta\theta$ (degree)	
	gold	gold-Chi/Napht	gold	gold-Chi/Napht
0	53.832	53.848	0	0
5	53.832	53.840	0	0.008
10	53.832	53.832	0	0.016
50	53.832	53.760	0	0.088
100	53.832	53.713	0	0.140
200	53.832	53.688	0	0.160
500	53.832	53.636	0	0.212
1000	53.832	53.561	0	0.287

© COPYRIGHT UPM

Table 4.3 it shows that there are no changes in resonance angle ($\Delta\theta = 0$) for all different glucose solutions in contact with bare gold thin film meanwhile for gold-Chi/Napht thin film the value of $\Delta\theta$ increased as the concentration of glucose increased. This can be attributed to increased of reflective index of sensing region when glucose molecule successfully binds with Chi/Napht thin film (Rosddi et al., 2021).

A graph of resonance angle shift, $\Delta\theta$ against concentration of glucose was plotted to obtained linear regression graph as shown in Figure 4.9. Ths graph can further explain the sensitivity of gold and gold-Chi/Napht thin film towards 0-1000 nM concentration of glucose.

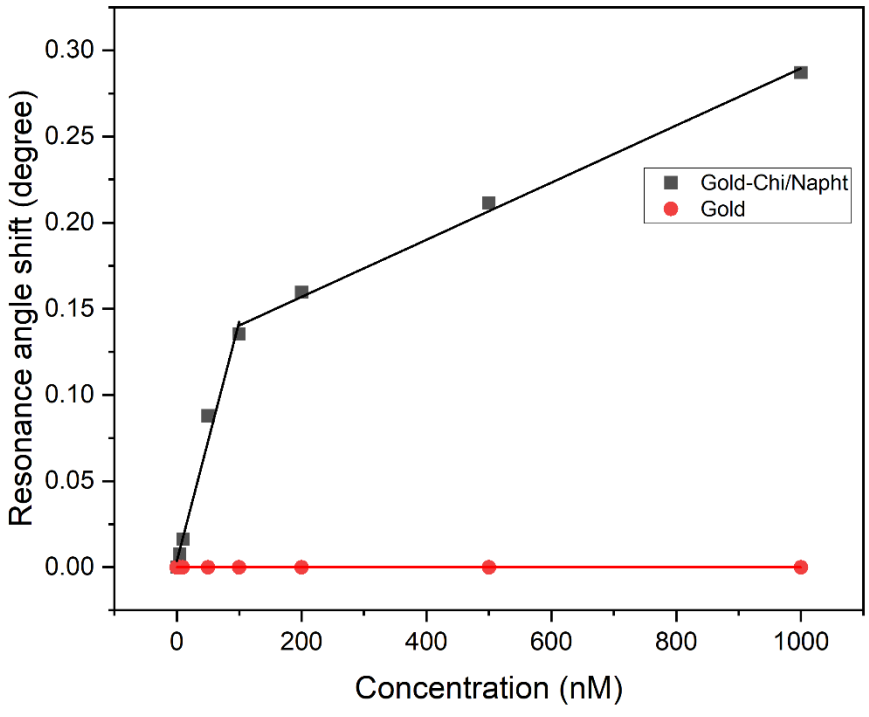

Figure 4.9: The resonance angle shift of gold and Chi/Napht thin film in contact with different glucose concentration.

For gold-Chi/Napht thin films, two different regions were fitted separately in order to achieve the best linear fit regression R^2 as shown in Figure 4.9. The first region and second region are from 0 to 100 nM and 200 to 1000 nM, respectively. Linear regression coefficient R^2, linear regression analysis and the equation represented relationship between SPR angle shift (Δθ SPR) and the glucose concentration were obtained for each region. For the first region the value of linear regression coefficient was 0.97203 and the relationship between the SPR angle shift (Δθ SPR) and glucose concentrations governed by the Eq. was $\Delta\theta\ SPR = 1.0014[glucose] + 1.1743 \times 10^{-4}$ Meanwhile for the second region the value of R^2 was 0.99321 and $\Delta\theta\ SPR = 1.6578 \times 10^{-4}$ [glucose] + 7.9024×10^{-6} respectively. Linear regression gradient analysis was 1.0014° nM^{-1} and $1.6578° \times 10^{-4}$ nM^{-1} for first region and second region. The gradient of linear regression can be defined as the sensitivity of gold-Chi/Napht thin film towards glucose. Therefore, it can be concluded that gold-Chi/Napht thin film was sensitive toward glucose and exhibited more sensitivity for lower concentration of glucose.

4.5 Atomic Force Microscopy

The microscopic of Chi/Napht thin film was studied by using atomic force microscopy (AFM) that works in tapping mode. The scan size of 10 μm × 10 μm was used in order to get the most precise images in two dimension (2D) and three dimension (3D). Figure 4.10 shows AFM image of Chi/Napht thin film before and after in in contact with glucose solution. The RMS roughness value and surface morphology value for all thin films were obtained by using AFM.

© COPYRIGHT UPM

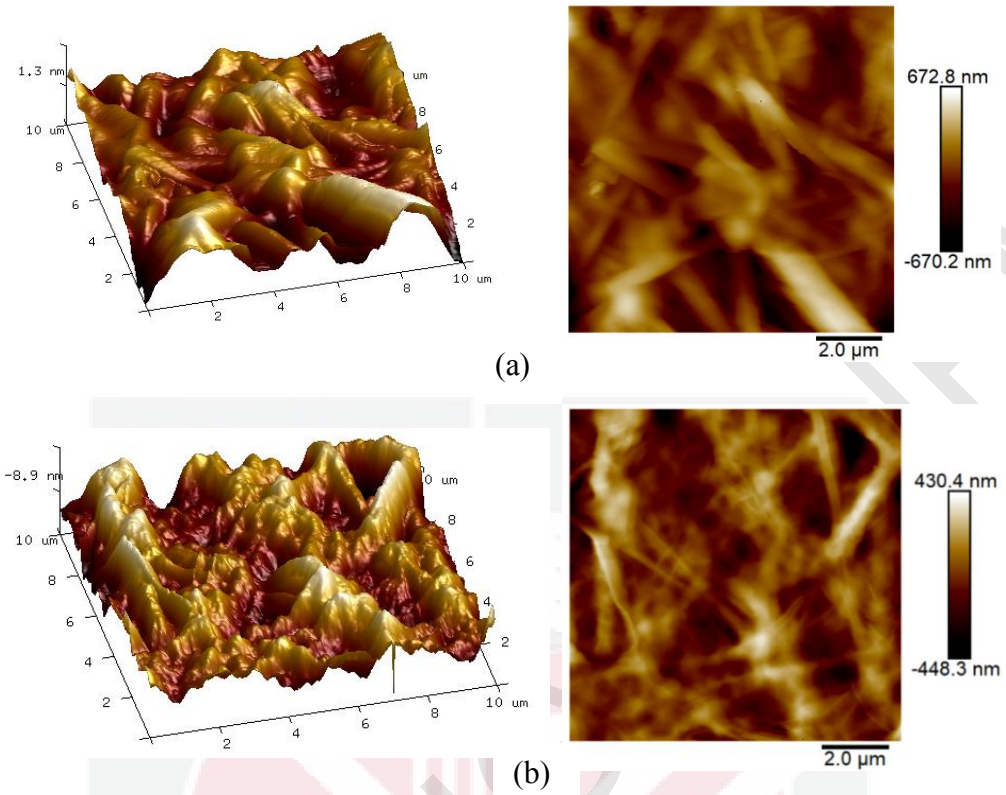

Figure 4.10: AFM image of Chi/Napht (a) before and (b) after in contact with glucose solution.

RMS roughness for Chi/Napht thin film before and after contact with glucose solution are 0.179 and 0.125 µm respectively. The reduction of the surface roughness value for Chi/Napht after in contact probably due to glucose absorption by Chi/Napht which resulting in a smoother surface of Chi/Napht thin film after in contact with glucose (Daniyal et al., 2018).

© COPYRIGHT UPM

CHAPTER 5

CONCLUSION

5.1 Conclusion

The first aim of these studies was to identify the structural and optical properties of chitosan-1,8-naphthalimide (Chi/Napht). The structural properties of Chi/Napht were successfully studied using Fourier transform infrared spectroscopy (FTIR) and atomic force microscopy (AFM). While for optical properties of Chi/Napht was characterized by using UV-visible spectroscopy (UV-Vis). The second aim of these studies was to determine the potential of Chi/Napht in glucose sensing using surface plasmon resonance (SPR) optical sensor.

The FTIR result has successfully determined the functional group excited in Chi/Napht. The result showed the peak at 1700.67 cm^{-1}, 2826.71 cm^{-1}, 113.25 cm^{-1} indicated the present of carboxyl group (COOH), methylene group (C−H) and carbonyl group (C−O) for each peak. While the other two peaks appeared at 865.99 cm^{-1} and 870.72 cm^{-1} due to benzene ring of 1,8-naphthalimide. The last peak in these studies was at 556.53 cm^{-1} indicated the C−C stretching bond of naphthalene ring.

Next, UV-Vis has successfully used identified the energy band gap and absorbance value of chitosan, 1,8-naphthalimide and Chi/Napht thin film. Energy band gap for Chi/Napht was 3.978 eV, the lowest value compared to other thin film which 4.113 eV for chitosan and 4.098 eV for 1,8-napthalimide. The lowest energy band gap of Chi/Napht was due to the strongest interatomic spacing between atom of Chi/Napht that caused high energy needed to move the electron. Meanwhile the absorbance value

© COPYRIGHT UPM

for chitosan, 1,8-naphthalimide and Chi/Napht thin film were 3.82 at peak 281 nm, 4.0 at peak 276.18 nm and 2.61 at peak 287.54 nm respectively.

The sensing properties of the Chi/Napht thin film in glucose sensing has been sucessfull investigated using SPR. The SPR result for gold thin film and gold-Chi/Napht thin film in detect glucose were compared. It shows that gold-Chi/Napht thin film can produce positive responses for different concentration of glucose injected. From linear regression graph, the gradient of was 1.0014° nM^{-1} and 1.6578° $\times 10^{-4}$ nM^{-1} for the glucose concentration range of 5 to 100 nM and 200 to 1000 nM, respectively. The lowest detection limit obtained in these studies for Chi/Napht thin film in glucose detection was as low as 5 nM.

Lastly, AFM has sucessully studied on surface morphology of Chi/Napth thin film before contact and after in contact with glucose solution. The result showed roughness value for before contact was 0.179 μm and for after contact was 0.125 μm.

Based on the finding from these studies it can be concluded that Chi/Napht thin film has been successful synthesized. It also proved that Chi/Napht thin film has goof potential in detect glucose solution using SPR method. Therefore, this study may provide good contribution to the society whereas it can be applied in wide range of sensor applications.

5.2 Recommendation for Future Work

To further improve this work, the structural and optical properties of Chi/Napht thin film can be studied on more details by using various method. For optical properties, the example of method is photoluminescence to study on the discrete energy level as well as emission of wavelength. Next, detection of different type of

© COPYRIGHT UPM

carbohydrates such as fructose, sucrose and galactose can also be done in future studies. Last but not least future work on studying other material can be interesting to enhance the sensitivity and selectivity of the sensor.

© COPYRIGHT UPM

REFERENCES

Banerjee, S., Veale, E. B., Phelan, C. M., Murphy, S. A., Tocci, G. M., Gillespie, L. J., Frimannsson, D. O., Kelly, J. M., & Gunnlaugsson, T. (2013). Recent advances in the development of 1,8-naphthalimide based DNA targeting binders, anticancer and fluorescent cellular imaging agents. *Chemical Society Reviews*, *42*(4), 1601–1618. https://doi.org/10.1039/c2cs35467e

Bojinov, V., & Grabchev, I. (2003). Synthesis of new polymerizable 1,8-naphthalimide dyes containing a 2-hydroxyphenylbenzotriazole fragment. *Dyes and Pigments*, *59*(3), 277–283. https://doi.org/10.1016/S0143-7208(03)00113

Bourigua, S., Maaref, A., Bessueille, F., & Renault, N. J. (2013). A new design of electrochemical and optical biosensors based on biocatalytic growth of Au nanoparticles. *Electroanalysis*, *25*(3), 644–651. https://doi.org/10.1002/elan.201200243

Chen, Y., & Ming, H. (2012). Review of surface plasmon resonance and localized surface plasmon resonance sensor. *Photonic Sensors*, *2*(1), 37–49. https://doi.org/10.1007/s13320-011-0051-2

Dai, H., Wu, X., Xu, H., Wang, Y., Chi, Y., & Chen, G. (2009). A highly performing electrochemiluminescent biosensor for glucose based on a polyelectrolyte-chitosan modified electrode. *Electrochimical Acta*, *54*(19), 4582–4586. https://doi.org/10.1016/j.electacta.2009.03.042

Daniyal, W. M. E. M. M., Fen, Y. W., Abdullah, J., Saleviter, S., & Sheh Omar, N. A. (2018). Preparation and characterization of hexadecyltrimethylammonium bromide modified nanocrystalline cellulose/graphene oxide composite thin film and its potential in sensing copper ion using surface plasmon resonance technique. *Optik*, *173*, 71–77. https://doi.org/10.1016/j.ijleo.2018.08.014

© COPYRIGHT UPM

Fauzi, N. I. M., Fen, Y. W., Omar, N. A. S., Saleviter, S., Daniyal, W. M. E. M. M., Hashim, H. S., & Nasrullah, M. (2020). Nanostructured chitosan/maghemite composites thin film for potential optical detection of mercury ion by surface plasmon resonance investigation. *Polymers*, *12*(7), 1–13. https://doi.org/10.3390/polym12071497

Fen, Y. W., Yunus, W. M. M., Yusof, N. A., Ishak, N. S., Omar, N. A. S., & Zainudin, A. A. (2015). Preparation, characterization and optical properties of ionophore doped chitosan biopolymer thin film and its potential application for sensing metal ion. *Optik*, *126*(23), 4688–4692. https://doi.org/10.1016/j.ijleo.2015.08.098

Fen, Y. W., Yunus, W. M. M., & Yusof, N. A. (2012). Surface plasmon resonance optical sensor for detection of Pb^{2+} based on immobilized p-tert-butylcalix[4] arene-tetrakis in chitosan thin film as an active layer. *Sensors and Actuators*, *B: Chemical*, *171–172*, 287–293. https://doi.org/10.1016/j.snb.2012.03.070

Fu, Y., & Finney, N. S. (2018). Small-molecule fluorescent probes and their design. *RSC Advances*, *8*(51), 29051–29061. https://doi.org/10.1039/c8ra02297f

Fu, Y., Pang, X. X., Wang, Z. Q., Qu, H. T., & Ye, F. (2018). Synthesis and fluorescent property study of novel 1,8-naphthalimide-based chemosensors. *Molecules*, *23*(2), 1–14. https://doi.org/10.3390/molecules23020376

Galed, G., Miralles, B., Panos, I., Santiago, A., Heras, A. (2005). N-deacetylation and depolymerization of chitin/chitosan: influence of the source of chitin. *Carbohydrate Polymers*, *62*, 316−320. https://doi.org/10.1016/j.carbpol.2005.03.019

Gasti, T., Hiremani, V. D., Sataraddi, S. P., Vanjeri, V. N., Goudar, N., Masti, S. P., Chougale, R. B., & Malabadi, R. B. (2021). UV screening, swelling and in-vitro

© COPYRIGHT UPM

cytotoxicity study of novel chitosan/poly (1-vinylpyrrolidone-co-vinyl acetate) blend films. *Chemical Data Collections*, *33*, 100684. https://doi.org/10.1016/j.cdc.2021.100684

Geddes, R. (1969). Starch biosynthesis. *Quarterly Reviews and Chemical Society*, *23*(1), 57–72. https://doi.org/10.1039/qr9692300057

Geraghty, C., Wynne, C., & Elmes, R. B. P. (2021). 1,8-naphthalimide based fluorescent sensors for enzymes. *Coordination Chemistry Reviews*, *437*, 213713. https://doi.org/10.1016/j.ccr.2020.213713

Ghosh, J., Ghosh, R., & Giri, P. K. (2018). Tuning the visible photoluminescence in Al doped ZnO thin film and its application in label-free glucose detection. *Sensors and Actuators*, *B: Chemical*, *254*, 681–689. https://doi.org/10.1016/j.snb.2017.07.110

Ghosh, R., Das, R., & Giri, P. K. (2018). Label-free glucose detection over a wide dynamic range by mesoporous Si nanowires based on anomalous photoluminescence enhancement. *Sensors and Actuators*, *B: Chemical*, *260*, 693–704. https://doi.org/10.1016/j.snb.2018.01.099

Grabchev, I., Petkov, C., & Bojinov, V. (2001). Synthesis and absorption properties of some new bis-1,8-naphthalimides. *Dyes and Pigments*, *48*(3), 239–244. https://doi.org/10.1016/S0143-7208(00)00109-1

Gupta, R., Ghosh, A., Singh, A. K., & Misra, A. (2020). Clinical considerations for patients with diabetes in times of COVID-19 epidemic. *Diabetes and Metabolic Syndrome: Clinical Research and Reviews*, *14*(3), 211–212. https://doi.org/10.1016/j.dsx.2020.03.002

He, L., Liu, Q., Zhang, S., Zhang, X., Gong, C., Shu, H., Wang, G., Liu, H., Wen, S., & Zhang, B. (2018). High sensitivity of TiO_2 nanorod array electrode for

© COPYRIGHT UPM

photoelectrochemical glucose sensor and its photo fuel cell application. *Electrochemistry Communications*, *94*, 18–22. https://doi.org/10.1016/j.elecom.2018.07.021

Hossain, M. F., & Park, J. Y. (2016). Plain to point network reduced graphene oxide-activated carbon composites decorated with platinum nanoparticles for urine glucose detection. *Scientific Reports*, *6*. https://doi.org/10.1038/srep21009

Jia, X., Yang, Y., Xu, Y., & Qian, X. (2014). Naphthalimides for labeling and sensing applications. *Pure and Applied Chemistry*, *86*(7), 1237–1246. https://doi.org/10.1515/pac-2013-1025

Jiang, H., Chen, Z., Cao, H., & Huang, Y. (2012). Peroxidase-like activity of chitosan stabilized silver nanoparticles for visual and colorimetric detection of glucose. *Analyst*, *137*(23), 5560–5564. https://doi.org/10.1039/c2an35911a

Jiang, J., Chen, D., & Du, X. (2017). Electrochemiluminescence sensing platform for sensitive glucose detection based on in situ generation and conversion of coreactants. *Sensors and Actuators*, *B: Chemical*, *251*, 256–263. https://doi.org/10.1016/j.snb.2017.05.066

Juska, V. B., & Pemble, M. E. (2020). A critical review of electrochemical glucose sensing: evolution of biosensor platforms based on advanced nanosystems. *Sensors*, *20*(21), 1–28. https://doi.org/10.3390/s20216013

Kumar, S., Nigam, N., Ghosh, T., Dutta, P. K., Singh, S. P., Datta, P. K., An, L., & Shi, T. F. (2010). Preparation, characterization and optical properties of a novel azo-based chitosan biopolymer. *Materials Chemistry and Physics*, *120*(2–3), 361–370. https://doi.org/10.1016/j.matchemphys.2009.11.018

Li, D., Su, J., Yang, J., Yu, S., Zhang, J., Xu, K., & Yu, H. (2017). Optical surface plasmon resonance sensor modified by mutant glucose/galactose-binding protein

© COPYRIGHT UPM

for affinity detection of glucose molecules. *Biomedical Optics Express*, *8*(11), 5206. https://doi.org/10.1364/boe.8.005206

Liang, B., Wang, B., Ma, Q., Xie, C., Li, X., & Wang, S. (2018). A lysosome-targetable turn-on fluorescent probe for the detection of thiols in living cells based on a 1,8-naphthalimide derivative. *Spectrochimica Acta*, *A: Molecular and Biomolecular Spectroscopy*, *192*, 67–74. https://doi.org/10.1016/j.saa.2017.10.044

Lidiya, A. E., Raja, R. V. J., Pham, V. D., Ngo, Q. M., & Vigneswaran, D. (2019). Detecting hemoglobin content blood glucose using surface plasmon resonance in D-shaped photonic crystal fiber. *Optical Fiber Technology*, *50*, 132–138. https://doi.org/10.1016/j.yofte.2019.03.009

Lin, L., Song, X., Chen, Y., Rong, M., Zhao, T., Wang, Y., Jiang, Y., & Chen, X. (2015). Intrinsic peroxidase-like catalytic activity of nitrogen-doped graphene quantum dots and their application in the colorimetric detection of H_2O_2 and glucose. *Analytica Chimica Acta*, *869*, 89–95. https://doi.org/10.1016/j.aca.2015.02.024

Lobry, M., Lahem, D., Loyez, M., Debliquy, M., Chah, K., David, M., & Caucheteur, C. (2019). Non-enzymatic D-glucose plasmonic optical fiber grating biosensor. *Biosensors and Bioelectronics*, *142*, 111506. https://doi.org/10.1016/j.bios.2019.111506

Lou, F., Lu, Z., Hu, F., & Ming, C. (2017). A 3D bio-platform constructed by glucose oxidase adsorbed on Au nanoparticles assembled polyaniline nanowires to sensitively detect glucose by electrochemiluminescence. *Journal of Electroanalytical Chemistry*, *787*, 125–131. https://doi.org/10.1016/j.jelechem.2017.01.048

© COPYRIGHT UPM

Lu, Q., Huang, T., Zhou, J., Zeng, Y., Wu, C., Liu, M., Li, H., Zhang, Y., & Yao, S. (2021). Spectroscopy limitation-induced fluorescence enhancement of carbon nanoparticles and their application for glucose detection. *Spectrochimica Acta*, *A: Molecular and Biomolecular Spectroscopy*, *244*, 118893. https://doi.org/10.1016/j.saa.2020.118893

Mai, H. H., Tran, D. H., & Janssens, E. (2019). Non-enzymatic fluorescent glucose sensor using vertically aligned ZnO nanotubes grown by a one-step, seedless hydrothermal method. *Microchimica Acta*, *186*(4), 1–10. https://doi.org/10.1007/s00604-019-3353-5

Marie, M., Mandal, S., & Manasreh, O. (2015). An electrochemical glucose sensor based on zinc oxide nanorods. *Sensors*, *15*(8), 18714–18723. https://doi.org/10.3390/s150818714

Maruthupandy, M., Rajivgandhi, G., Muneeswaran, T., Vennila, T., Quero, F., & Song, J. M. (2019). Chitosan/silver nanocomposites for colorimetric detection of glucose molecules. *International Journal of Biological Macromolecules*, *121*, 822–828. https://doi.org/10.1016/j.ijbiomac.2018.10.063

Menon, P. S., Mulyanti, B., Jamil, N. A., Wulandari, C., Nugroho, H. S., Mei, G. S., Zainul Abidin, N. F., Hasanah, L., Pawinanto, R. E., & Berhanuddin, D. D. (2019). Refractive index and sensing of glucose molarities determined using Au-Cr K-SPR at 670/785 nm wavelength. *Sains Malaysiana*, *48*(6), 1259–1265. https://doi.org/10.17576/jsm-2019-4806-13

Mukhtar, W. M., Ayob, N. R., Halim, R. M., Samsuri, N. D., Murat, N. F., Rashid, A. R. A., & Dasuki, K. A. (2018). Effect of noble metal thin film thicknesses on surface plasmon resonance (SPR) signal amplification. *Journal of Advanced*

© COPYRIGHT UPM

Research in Materials Science, *49*(1), 1–9. https://doi.org/www.akademiabaru.com/arms.html

Nie, J., Zhang, J., Bei, J., & Chen, G. (2008). Optical properties of zinc barium silicate glasses. *Journal of Non-Crystalline Solids*, *354*(12–13), 1361–1364. https://doi.org/10.1016/j.jnoncrysol.2006.11.042

Nosal, W. H., Thompson, D. W., Yan, L., Sarkar, S., Subramanian, A., & Woollam, J. A. (2005). UV-vis-infrared optical and AFM study of spin-cast chitosan films. *Colloids and Surfaces B: Biointerfaces*, *43*(3–4), 131–137. https://doi.org/10.1016/j.colsurfb.2004.08.022

Oh, J. W., Chun, S. C., & Chandrasekaran, M. (2019). Preparation and in vitro characterization of chitosan nanoparticles and their broad-spectrum antifungal action compared to antibacterial activities against phytopathogens of tomato. *Agronomy*, *9*(1), 21. https://doi.org/10.3390/agronomy9010021

Pattnaik, P. (2005). Surface plasmon resonance: applications in understanding receptor-ligand interaction. *Applied Biochemistry and Biotechnology*, *126*(2), 79–92. https://doi.org/10.1385/abab:126:2:079

Phan, Q. H., Lai, Y. R., Xiao, W. Z., Pham, T. T. H., & Lien, C. H. (2020). Surface plasmon resonance prism coupler for enhanced circular birefringence sensing and application to non- invasive glucose detection. *Optics Express*, *28*(17), 24889. https://doi.org/10.1364/oe.400721

Prabowo, B. A., Purwidyantri, A., & Liu, K. C. (2018). Surface plasmon resonance optical sensor: a review on light source technology. *Biosensors*, *8*(3). https://doi.org/10.3390/bios8030080

Refat, M. S., Ismail, L. A., & Adam, A. M. A. (2015). Shedding light on the photostability of two intermolecular charge-transfer complexes between highly

© COPYRIGHT UPM

fluorescent bis-1,8-naphthalimide dyes and some π-acceptors: a spectroscopic study in solution and solid states. *Spectrochimica Acta*, *A: Molecular and Biomolecular Spectroscopy*, *134*, 288–301. https://doi.org/10.1016/j.saa.2014.06.107

Ren, B., Yang, Y., Qu, Y., Cao, J., & Wu, Y. (2019). Two fluorophore compounds based on 1, 8-naphthalimide: synthesis, crystal structure, and optical properties. *Journal of Molecular Structure*, *1193*, 131–140. https://doi.org/10.1016/j.molstruc.2019.04.130

Rinaudo, M. (2006). Chitin and chitosan: properties and applications. *Progress in Polymer Science*, *31*(7), 603–632. https://doi.org/10.1016/j.progpolymsci.2006.06.001

Rosddi, N. N. M., Fen, Y. W., Omar, N. A. S., Anas, N. A. A., Hashim, H. S., Ramdzan, N. S. M., Fauzi, N. I. M., Anuar, M. F., & Daniyal, W. M. E. M. M. (2021). Glucose detection by gold modified carboxyl-functionalized graphene quantum dots-based surface plasmon resonance. *Optik*, *239*. https://doi.org/10.1016/j.ijleo.2021.166779

Seraj, S., Rouhani, S., & Faridbod, F. (2019). Naphthalimide-based optical turn-on sensor for monosaccharide recognition using boronic acid receptor. *RSC advances*, *9*(31), 17933–17940. https://doi.org/10.1039/c9ra01757

Sharma, A., & Kumar, A. (2016). Study of structural and electro-catalytic behaviour of amperometric biosensor based on chitosan/polypyrrole nanotubes-gold nanoparticles nanocomposites. *Synthetic Metals*, *220*, 551–559. https://doi.org/10.1016/j.synthmet.2016.07.012

Shen, Y., Zhang, X., Huang, X., Zhang, Y., Zhang, C., Jin, J., Liu, X., Li, H., & Yao, S. (2015a). A new fluorescence and colorimetric sensor for highly selective and

© COPYRIGHT UPM

sensitive detection of glucose in 100% water. *RSC Advances*, *5*(78), 63226–63232. https://doi.org/10.1039/c5ra11116a

Shendurse, A. M., & Khedkar, C. D. (2015). Glucose: properties and analysis. *In Encyclopedia of Food and Health*, *3*, 239−247. https://doi.org/10.1016/B978-0-12-384947-2.00353-6

Singh, P. K., Bhattacharya, B., Nagarale, R. K., Kim, K. W., & Rhee, H. W. (2010). Synthesis, characterization and application of biopolymer-ionic liquid composite membranes. *Synthetic Metals*, *160*(1–2), 139–142. https://doi.org/10.1016/j.synthmet.2009.10.021

Srivastava, S. K., Verma, R., & Gupta, B. D. (2012). Surface plasmon resonance based fiber optic glucose biosensor. *Third Asia Pacific Optical Sensors Conference*, *8351*, 451−456. https://doi.org/10.1117/12.915978

Sun, Y., Liang, X., Fan, J., & Han, Q. (2013). Studies on the photophysical properties of 1,8-naphthalimide derivative and aggregation induced emission recognition for casein. *Journal of Luminescence*, *141*, 93–98. https://doi.org/10.1016/j.jlumin.2013.02.053

Tian, L., Qiu, J., Zhou, Y. C., & Sun, S. G. (2010). Application of polypyrrole/GOx film to glucose biosensor based on electrochemical-surface plasmon resonance technique. *Microchimica Acta*, *169*(3), 269–275. https://doi.org/10.1007/s00604-010-0344-y

Usman, F., Dennis, J. O., Ahmed, A. Y., Meriaudeau, F., Ayodele, O. B., & Rabih, A. A. S. (2018). A review of biosensors for non-invasive diabetes monitoring and screening in human exhaled breath. *IEEE Access*, *7*, 5963–5974. https://doi.org/10.1109/ACCESS.2018.2887066

© COPYRIGHT UPM

Uwimbabazi, E., Mukasekuru, M. R., & Sun, X. (2017). Glucose biosensor based on a glassy carbon electrode modified with multi-walled carbon nanotubes-chitosan for the determination of beef freshness. *Food Analytical Methods*, *10*(8), 2667–2676. https://doi.org/10.1007/s12161-017-0793-6

Wang, B., Koo, B., & Monbouquette, H. G. (2017). Enzyme deposition by polydimethylsiloxane stamping for biosensor fabrication. *Electroanalysis*, *29*(10), 2300–2306. https://doi.org/10.1002/elan.201700302

Wang, D., Liang, Y., Su, Y., Shang, Q., & Zhang, C. (2019). Sensitivity enhancement of cloth-based closed bipolar electrochemiluminescence glucose sensor via electrode decoration with chitosan /multi-walled carbon nanotubes/graphene quantum dots-gold nanoparticles. *Biosensors and Bioelectronic*, *130*, 55–64. https://doi.org/10.1016/j.bios.2019.01.027

Wang, S., Li, S., Wang, W., Zhao, M., & Liu, J. (2019). Chemical non-enzymatic photoelectrochemical glucose sensor based on $BiVO_4$ electrode under visible light. *Sensor and Actuators*, *B: Chemical*, *291*, 34–41. https://doi.org/10.1016/j.snb.2019.04.057

Xie, J., Chen, Y., Yang, W., Xu, D., & Zhang, K. (2011). Water soluble 1,8-naphthalimide fluorescent pH probes and their application to bioimagings. *Journal of Photochemistry and Photobiology A: Chemistry*, *223*(2–3), 111–118. https://doi.org/10.1016/j.jphotochem.2011.08.006

Yu, S., Ding, L., Lin, H., Wu, W., & Huang, J. (2019). A novel optical fiber glucose biosensor based on carbon quantum dots-glucose oxidase/cellulose acetate complex sensitive film. *Biosensors and Bioelectronics*, *146*, 111760. https://doi.org/10.1016/j.bios.2019.111760

© COPYRIGHT UPM

Yuan, H., Ji, W., Chu, S., Qian, S., Wang, F., Masson, J. F., Han, X., & Peng, W. (2018). Fiber-optic surface plasmon resonance glucose sensor enhanced with phenylboronic acid modified Au nanoparticles. *Biosensors and Bioelectronics*, *117*, 637–643. https://doi.org/10.1016/j.bios.2018.06.042

Yuan, Y., Yang, X., Gong, D., Liu, F., Hu, W., Cai, W., Huang, J., & Yang, M. (2017). Investigation for terminal reflection optical fiber SPR glucose sensor and glucose sensitive membrane with immobilized GODs. *Optics Express*, *25*(4), 3884. https://doi.org/10.1364/oe.25.003884

Zhang, X. Y., Liu, S. G., Zhang, W. J., Wang, X. H., Han, L., Ling, Y., Li, N. B., & Luo, H. Q. (2019). Photoelectrochemical platform for glucose sensing based on g-C_3N_4/$ZnIn_2S_4$ composites coupled with bi-enzyme cascade catalytic in-situ precipitation. *Sensors and Actuators*, *B: Chemical*, *297*, 126818. https://doi.org/10.1016/j.snb.2019.126818

Zhang, Z., Lv, T., Tao, B., Wen, Z., Xu, Y., Li, H., Liu, F., & Sun, S. (2020). A novel fluorescent probe based on naphthalimide for imaging nitroreductase (NTR) in bacteria and cells. *Bioorganic and Medicinal Chemistry*, *28*(3), 115280. https://doi.org/10.1016/j.bmc.2019.115280

Zhao, C. S., Liu, X. L., Yang, M., Fang, J. Y., Zhang, J. J., & Liu, F. Q. (2009). The preparation of copolymerized fluorescent microspheres of styrene using detergent-free emulsion polymerization. *Dyes and Pigments*, *82*(2), 134–141. https://doi.org/10.1016/j.dyepig.2008.12.006

Zhou, T., Su, Z., Wang, X., Luo, M., Tu, Y., & Yan, J. (2021). Fluorescence detections of hydrogen peroxide and glucose with polyethyleneimine-capped silver nanoclusters. *Spectrochimica Acta*, *A: Molecular and Biomolecular Spectroscopy*, *244*, 118881. https://doi.org/10.1016/j.saa.2020.118881

© COPYRIGHT UPM